LOS ALAMOS SCIENTIFIC LABORATORY
of the
University of California

LOS ALAMOS • NEW MEXICO

Quarterly Status Report on

Plutonium-238 Space Electric Power Fuel Development Program

October 1-December 31, 1969

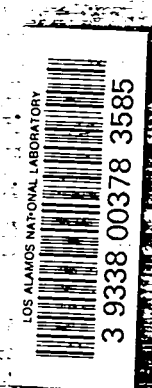

UNITED STATES
ATOMIC ENERGY COMMISSION
CONTRACT W-7405-ENG. 36

This LA...MS report presents the status of the Plutonium-238 Space Electric Power Fuel Development Program of Group CMB-11 of LASL.

LA-4068-MS
LA-4089-MS
LA-4328-MS

This report, like other special-purpose documents in the LA...MS series, has not been reviewed or verified for accuracy in the interest of prompt distribution.

Printed in the United States of America. Available from
Clearinghouse for Federal Scientific and Technical Information
National Bureau of Standards, U. S. Department of Commerce
Springfield, Virginia 22151
Price: Printed Copy $3.00; Microfiche $0.65

Distributed April 6, 1970

LA-4419-MS
UC-33, PROPULSION SYSTEMS
AND ENERGY CONVERSION
TID-4500

LOS ALAMOS SCIENTIFIC LABORATORY
of the
University of California
LOS ALAMOS • NEW MEXICO

Quarterly Status Report on

Plutonium-238 Space Electric Power Fuel Development Program

October 1-December 31, 1969

to

Space Isotopic Fuels and Materials Branch

Space Electric Power Office

Division of Space Nuclear Systems

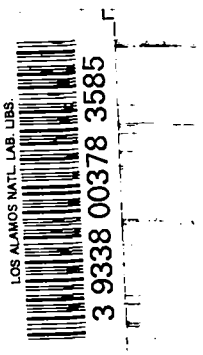

PROGRAM 07433

PLUTONIUM-238 SPACE ELECTRIC POWER FUEL DEVELOPMENT

Person in Charge: R.D. Baker

Principal Investigator: J.A. Leary

I. INTRODUCTION

Continuing studies have demonstrated the capability of forming $^{238}PuO_2$ containing solid solution cermets (SSC). Work during the previous quarter was primarily oriented toward procuring and installing proper equipment and toward establishing a process which would produce SSC material of the specified composition and power densities. The short time scale did not allow any significant amount of process development. However, the process flow sheet employed does yield SSC fuel with the desired properties.

Other studies have been in progress to characterize this fuel form and enough data have been obtained from these examinations to draw adequate conclusions as to its behavior and nature.

The fabrication of such a $^{238}PuO_2$-ThO_2-Mo cermet in the specified form of a 2.14 in. dia disc was achieved during this quarter. A schematic representation of such a standard disc is shown in Fig. 1. Table I lists common properties of a typical disc.

Table I

SELECTED PROPERTIES OF TYPICAL COATED SSC DISC

Property	Value
1. Weight	132 g
2. Volume	12.55 cc
3. Porosity	≤ 5%
4. Density	10.5 g/cc
5. Total Power	40 w
6. Power Density	3.2 w/cc
7. Specific Power	0.30 w/g

II. PROCESSING

An outline and general description of the process was given in the last Quarterly Report (LA-4238-MS) and overall details will not be repeated here. A status report on that process will be given in the following sections with appropriate illustrations wherever possible. For convenience, sections are organized in the same format as previous reports.

A. Preparation of Feed Material

No fundamental changes were instituted in this operation. A sufficient quantity of powder was always on hand to meet feed requirements. Table II lists average analysis of the last eight lots of incoming SRP material. These analyses are consistent with analytical reports for all material produced by SRP during FY 1969.

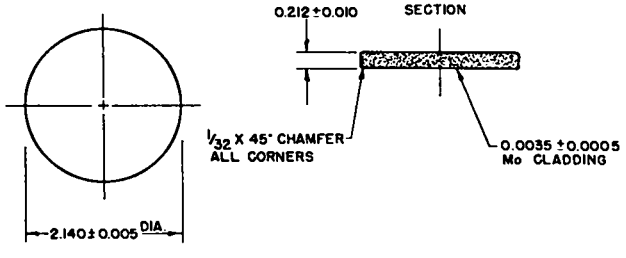

Fig. 1. Schematic of Typical SSC Disc showing dimensions, clad, and edge chamfer

Table II

AVERAGE SPECTROCHEMICAL ANALYSIS OF LAST EIGHT LOTS OF SRP $^{238}PuO_2$ FEED POWDER

Element	ppm by wt.	Element	ppm by wt.
Li	< 1	Ni	60
Be	< 1	Cu	8
B	2	Zn	< 20
Na	15	Sr	10
Mg	3	Ag	< 3
Al	30	Cd	< 5
Si	70	Sn	< 5
Ca	230	Pb	50
Cr	30	Bi	< 1
Mn	4	C	185
Fe	110		

This SRP $^{238}PuO_2$ is used without further purification and is blended with commercial 99.9% w/o ThO_2 powder.

Figure 2 shows a photomicrograph of a typical pressed and sintered disc prior to crushing and also a photograph of a 105-177μ size range particle batch after the crushing and screening. This material is now ready for Mo coating. A total of 711 g of feed powder in the stated size range was prepared during this quarter.

B. Coating of Powder

No significant changes in operating parameters were made in this step. Figure 3 is a photograph of the CVD coater in the ^{238}Pu facility. The soda-lime trap for HF off-gas is visible just above the coating device.

Some radiation studies were made on the effect of outgassing a typical lot of coated powder. Those results are discussed in Section II.D.9 below. A total of 570 g of feed powder was overcoated during this report period.

C. Hot Pressing

Figure 4 shows a photograph of the ^{238}Pu facility which houses the hot press. Figure 5 shows typical dies and punches used in these operations. Some of the hot pressing of small specimens involved the use of Ta liners in the die. Since a limited amount of Ta contamination was evident in the emission spectra of these specimens, no such liners have been used in the fabrication of the standard SSC discs.

Pressing parameters are essentially unchanged. Minor modifications in time-temperature-pressure conditions will be incorporated in the process as additional experience is gained from production of standard discs.

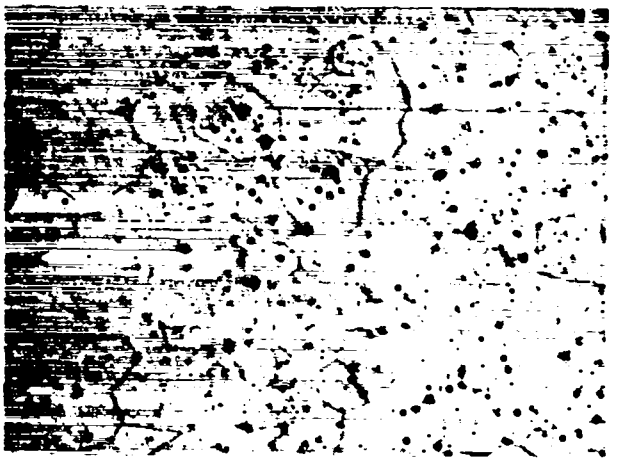

Sintered $^{238}PuO_2$-ThO_2 S.S. |10μ|

$^{238}PuO_2$-ThO_2 Particles |100μ|

Fig. 2. Photomicrograph of Sintered Ceramic and Resulting Crushed Powder

A total of 48 SSC specimens 0.25 in. dia x 0.25 high were fabricated during this quarter. In addition, several special 0.5 in. dia specimens were formed. The experience and technique attained during these preparations finally culminated in the synthesis of a standard 2.14 in. dia x 0.212 in. thick SSC disc. Fig. 6 is a photograph of that disc "as pressed".

D. Overcoating

A total of 44 specimens were overcoated with Mo. Some variations in coating parameters of time, flow rate of MoF_6, and temperature were investigated. Final resolution of conditions will depend on the results of overcoating the standard SSC discs. The internal heat from these discs as compared to the smaller specimens

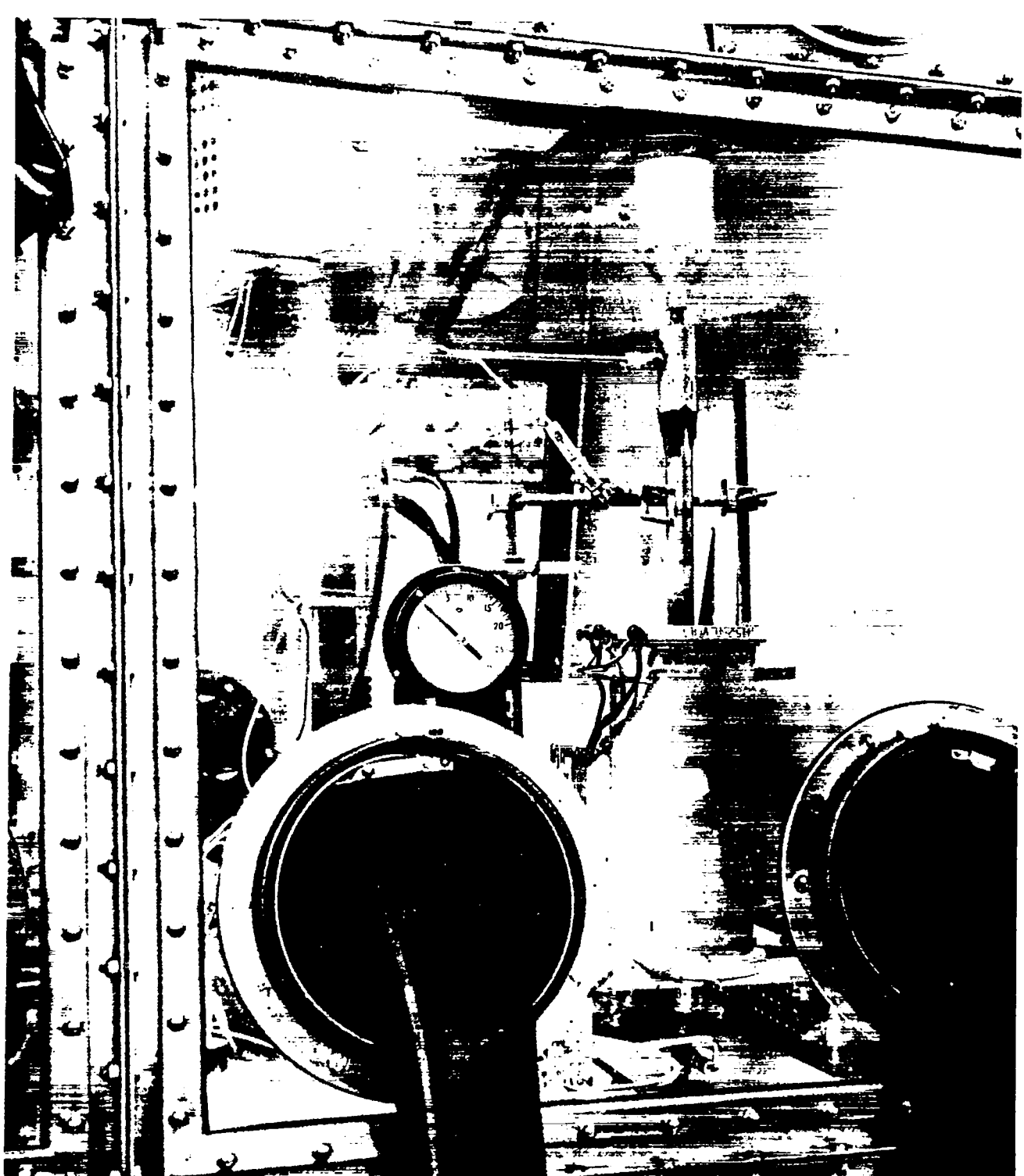

Figure 3. Particle Coater for CVD Coating of Feed Powder

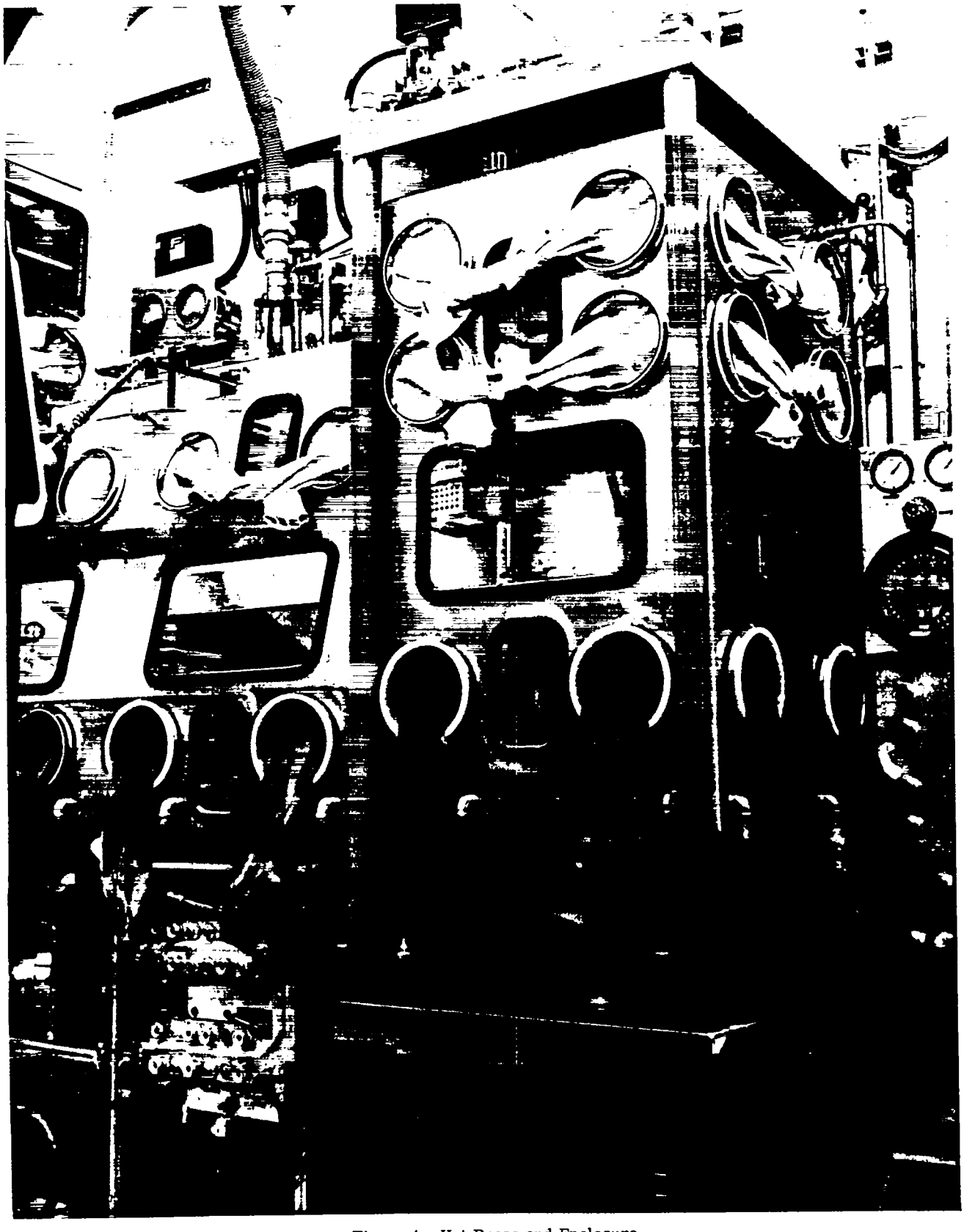

Figure 4. Hot Press and Enclosure

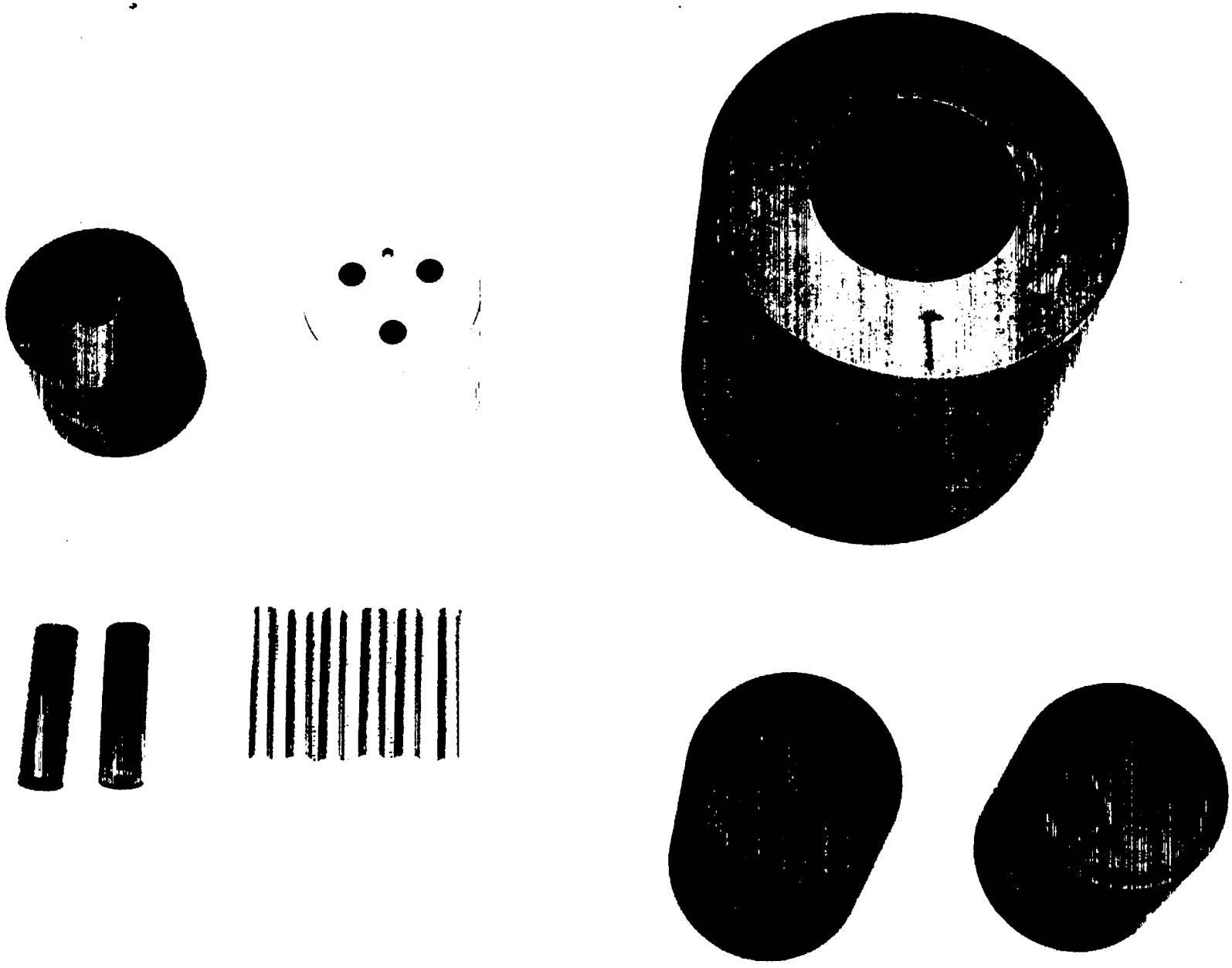

Figure 5. Dies and Punches Used in Hot Pressing

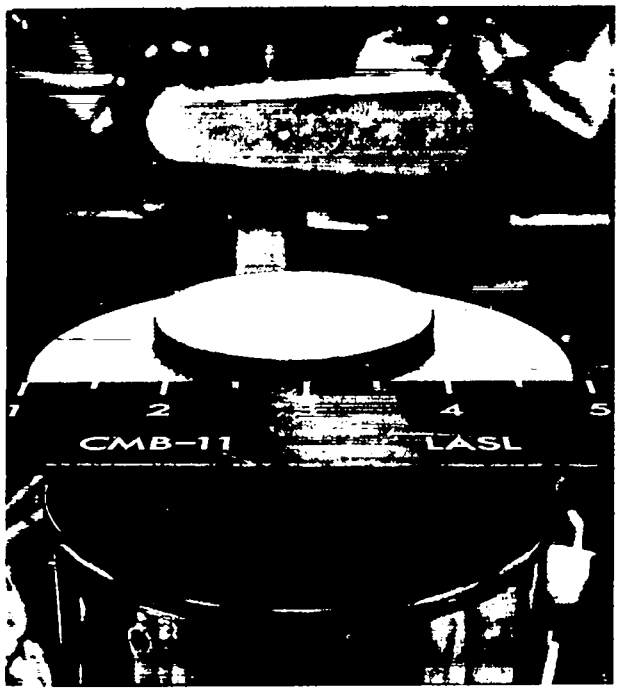

Figure 6. First "As Pressed" Standard SSC Disc

will undoubtedly be a factor affecting final coating conditions.

Figure 7 is a photograph of the barrel coater in a ^{238}Pu facility. Figure 8 is a photograph of a SSCS (solid solution cermet simulant) disc in the coater. The cushioning Mo springs insure that no extraneous metallic impurities or chips of the specimen are introduced.

Figure 8. SSCS (simulant) Disc Inside Barrel Coater

E. Machining

The Lorch lathe has been used in conjunction with a jeweler's lathe for machining SSC specimens. Figure 9 shows the Lorch lathe head and grinding attachment for trimming disc edges. Typical SSC machines rather slowly; however, chipping or spalling was not observed.

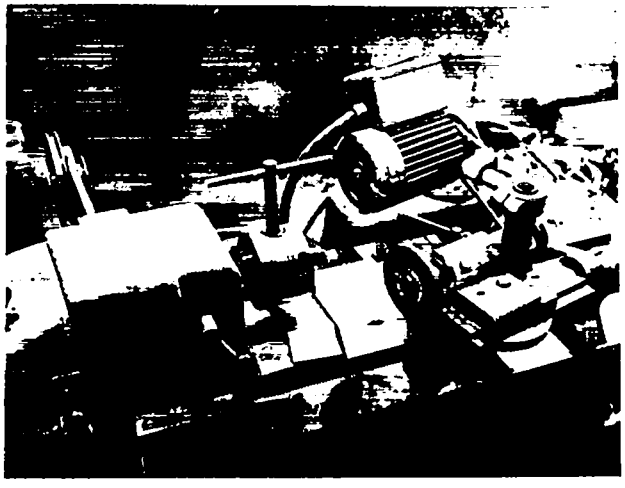

Figure 9. Lorch Lathe and Grinding Attachment

Figure 10 shows an example of machining and drilling as might be required for special purposes or tests.

III. PROPERTIES

A. Compatibility Testing:

The tungsten mesh furnace for compatibility testing in the 1500°C region is being installed and is expected to become operational in January, 1970.

A summary of the compatibility tests in progress is given in Table III. No new tests were started during the quarter; four tests were concluded and no gross reactions detected. On the basis of these tests, the following materials were found to be compatible with

Table III

COMPATIBILITY TEST PROGRAM SUMMARY
(December 16, 1969)

Capsule No.	Interfacial arrangement[a]	Test Conditions Temp. °C	Time to date (h)
HP-3 HP-4	$^{239}PuO_2$/TZM/$^{239}PuO_2$/TZM	1800	– 4500
HPT-2	$^{239}PuO_2$·53 ThO_2/TZM/$^{239}PuO_2$·53 ThO_2/TZM	1800	– 4500
HPT-3 HPT-5	$^{239}PuO_2$·56 ThO_2/TZM/$^{239}PuO_2$-56 ThO_2/TZM	1800	– 4500
LP-1 LP-2 LP-3	ThO_2/TZM/$^{239}PuO_2$-56 ThO_2/TZM/$^{239}PuO_2$	900	– 8000
LP-5	TZM/Pt-20 Rh/$^{239}PuO_2$/Pt-20 Rh/$^{239}PuO_2$-56 ThO_2/Pt-20 Rh/ThO_2/Pt-20 Rh/TZM	900	– 4600
LP-6	TZM/Pt-40 Rh/$^{239}PuO_2$/Pt-40 Rh/$^{239}PuO_2$·56 ThO_2/Pt-40 Rh/ThO_2/Pt-40 Rh/TZM	900	– 4600
LP-7	Mo/$^{239}PuO_2$-18 ThO_2/Ta-10 W/Mo/$^{239}PuO_2$-18 ThO_2/Ta-10 W/Mo	900	– 2600
LP-8	Mo/$^{239}PuO_2$·18 ThO_2/Ta-10 W/Mo	900	– 2600

[a] Compositions given in weight percent.

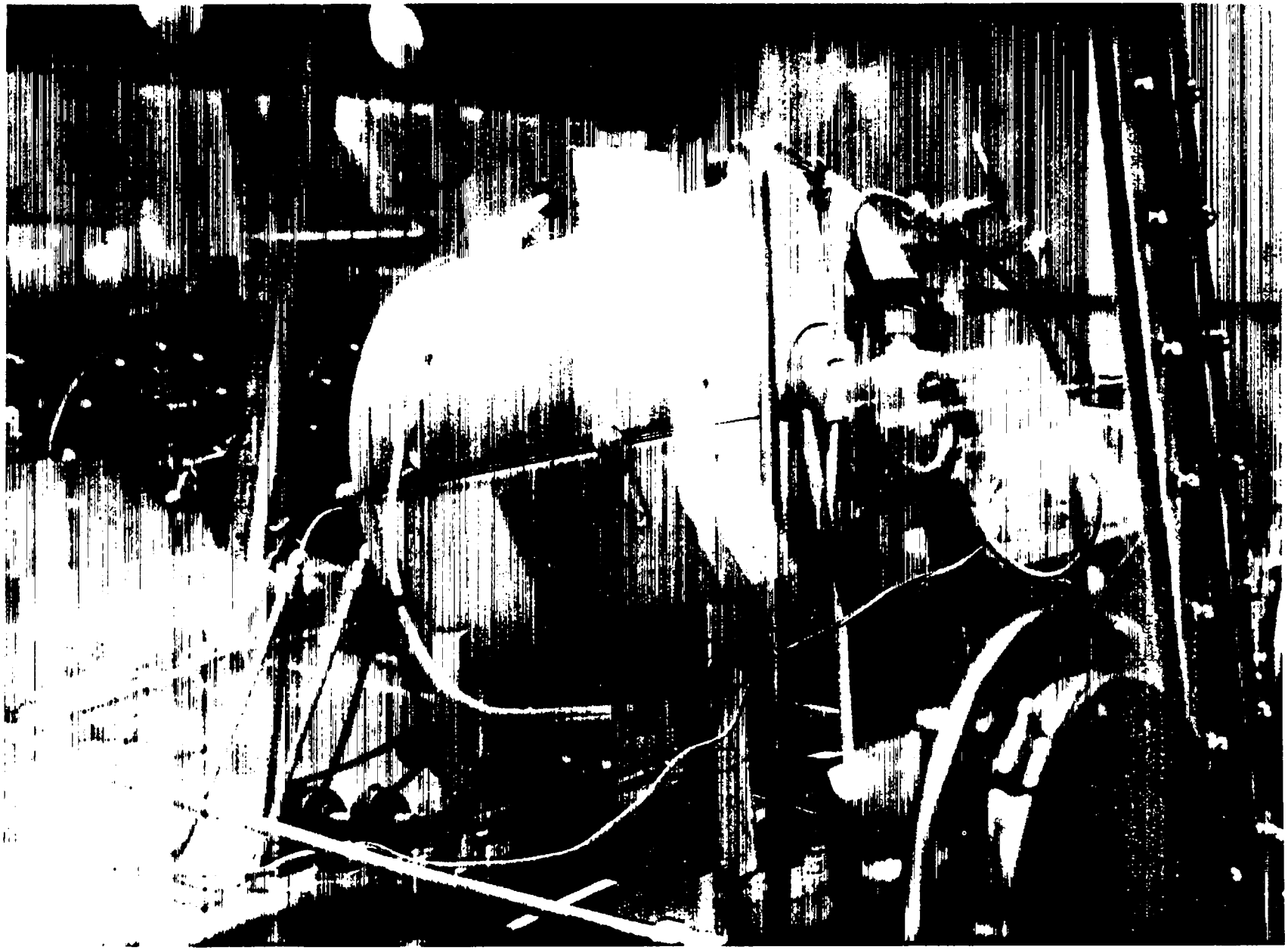

Figure 7. Barrel Coater for Overcoating SSC Discs

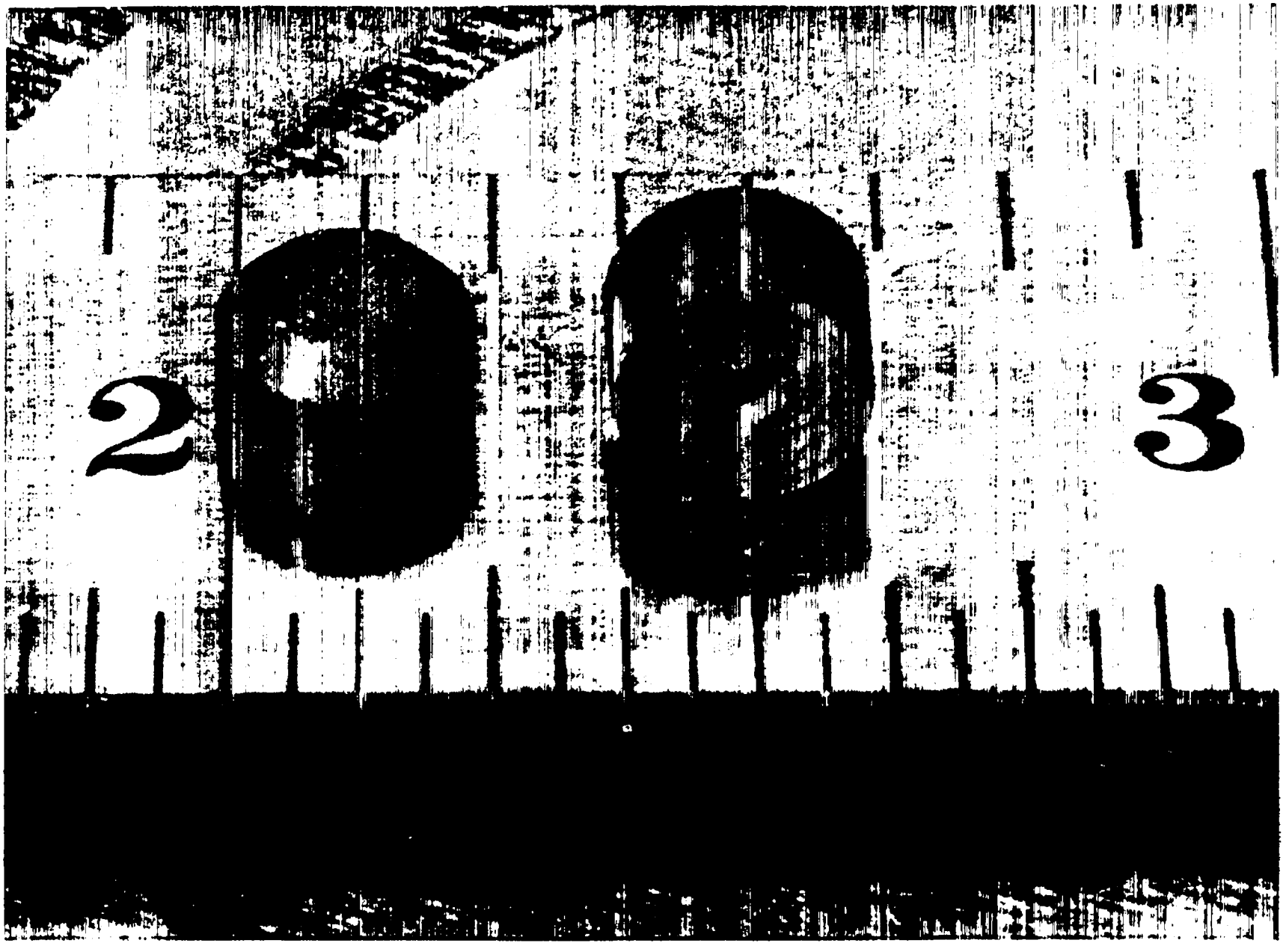

Figure 10. SSC Specimens Machined for Special Uses

TZM for the times and temperatures stated: $^{238}PuO_2$ for 1000 h at 1800°C; $^{238}PuO_2$-ZrO_2 solid solution for 6671 h at 900°C; and $^{238}PuO_2$-ThO_2 solid solution for 4910 h at 900°C and for 1000 h at 1800°C. The detailed results of the examinations are presented below.

Capsule HP-1, $^{238}PuO_2$ @ 1800°C.

Compatibility specimen HP-1 consisted of 100% $^{238}PuO_2$, 1/4 in. dia x 1/8 in. thick pellets in contact with TZM pellets. The mating faces of the pellets had been flattened on 600 grit SiC paper, and two pellets of each kind were held together within a heavy-walled TZM tube by a light molybdenum spring. The TZM tube was closed by TIG welding under approximately 1 in. Hg pressure of helium, and then was sealed within a tungsten capsule, which, in turn, was sealed within a Ta-10 w/o W alloy capsule to provide triple containment. The pellets, thus encapsulated, were heated for 1000 h at 1800°C at the Donald W. Douglas Laboratories and returned to LASL for examination.

After the outer two capsules had been removed in a glove box, the end of the TZM capsule containing the spring was cut off with a high-speed diamond cut-off wheel mounted on a Con-O-Saw. Freon TF was used as a coolant. The opened capsule was first filled with Epon 815 (epoxy) to pot the specimens and was then embedded in epoxy to facilitate handling during the sectioning operation. The capsule was sectioned longitudinally with the high-speed diamond saw, and both pieces were mounted for metallographic examination. Only one section of the specimen, however, was carried completely through the metallographic preparation procedures, which included rough grinding through 600 grit paper, polishing on a Syntron with 14.5 μm Al_2O_3 followed by Linde A, and etching the TZM with potassium ferricyanide.

The metallographic examination of this compatibility specimen included hardness testing. The hardness trace from the interface to the interior of the TZM pellet indicated no case hardening, and the average hardness, 218 VHN, was found to be comparable to that of a similar TZM specimen heated in vacuo for 24 h at 2000°C (211 VHN). Also, the microstructure of the TZM near the interface, see Fig. 11, appears to be

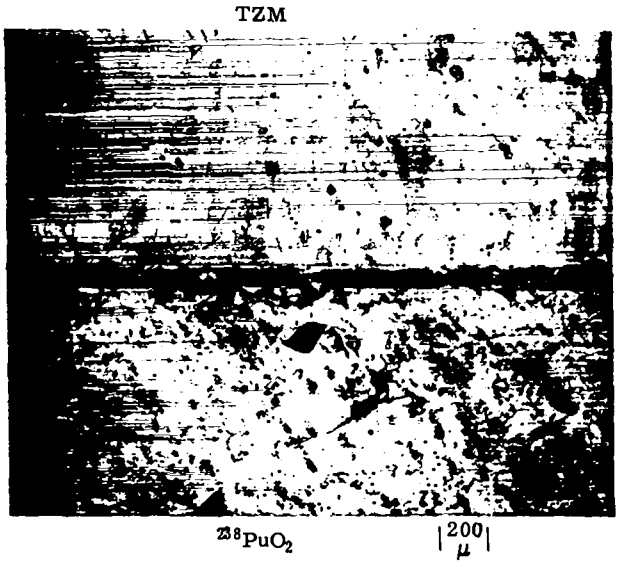

Fig. 11. TZM/$^{238}PuO_2$ Interface after 1000 h at 1800°C. TZM Etched with $K_3Fe(CN)_6$.

similar to that observed for TZM held in contact with $^{239}PuO_2$-49.4 w/o ThO_2 for 24 h at 2000°C. There appears to be a reaction layer extending to a depth of about 55 μm from the surface of the TZM, but electron microscopy of replicas taken from this area revealed the layer to be a very fine-grained region and not otherwise distinguishable from other areas in the TZM. In Fig. 11 there also appears to be a layer attached to the surface of the TZM. This layer has the same hardness, 847 VHN, as the $^{238}PuO_2$ matrix and appears to be $^{238}PuO_2$ which had become stuck to the TZM surface during heating and then had partially broken away from the pellet sometime after the test had been completed. Further evidence supporting this conclusion is the presence of bubbles (holes which extend to a depth of about 5 μm in the polished surface) just under the TZM surface. These bubbles, which have been identified as depressions in the surface by electron microscopy and which are shown in Fig. 15, were probably formed as a result of alpha particle bombardment of the TZM surface. The depth of the bubble filled layer suggests that the TZM surface did not recede significantly during the anneal. Also, the $^{238}PuO_2$ layer on the TZM mentioned above is shown at higher magnification in Fig. 12.

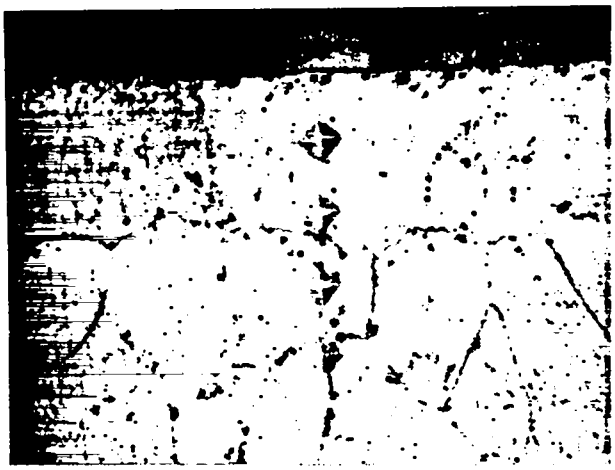

|20μ|

Fig. 12. Cross-section of a TZM Surface That Had Been in Contact with $^{238}PuO_2$ for 1000 h at 1800°C. $K_3Fe(CN)_6$ Etch.

The large number of precipitates seen in the TZM (see Fig. 12) is reminiscent of the microstructure of the TZM that was heated in contact with plutonia-thoria for 24 h at 2000°C. Since the $^{238}PuO_2$ in specimen HP-1 had lost considerable oxygen (it is clearly two-phase, see Fig. 11), it was first postulated that the precipitates were oxides. However, electron microprobe analysis has shown that the grain boundaries throughout the TZM contain more titanium, zirconium, and carbon than does the TZM matrix. Titanium X-ray intensities from these grain boundaries are as much as 30 to 100 times greater than those from the matrix areas removed from the PuO_2 contact surfaces. The TZM matrix within approximately 50 μm of the edges that were in contact with the PuO_2 contains less titanium and zirconium and more carbon than the unreacted matrix areas. Plutonium and oxygen were not detected in the TZM. This suggests that the grain boundary precipitates in the TZM are carbides -- probably complex carbides containing not only titanium and zirconium but also molybdenum. The source of the carbon is not known.

Molybdenum, titanium, and zirconium were not detected in the ceramic attached to the TZM. (Detection limits were estimated to be in the range between 0.01 and 0.05 percent.) This indicates that the attached material is PuO_2 that stuck to the TZM pellet during the anneal and then broke away from the pellet during subsequent handling.

The microstructure of the $^{238}PuO_2$ was revealed without etching, as seen in Figs. 11 and 13. The most interesting features can be seen in Fig. 13. Here, the individual grains are clearly delineated. Electron microscopy of replicas taken from this surface clearly indicated that the grain boundaries were largely empty and provided the explanation that the regular holes in the surface (see Fig. 13) were formed when whole grains were removed from the surface during metallographic polishing. The grain boundaries must indeed have acted as helium reservoirs in this material. Also shown in Fig. 13 are many large, irregular holes in the surface of the $^{238}PuO_2$ which were probably formed by the accumulation of both oxygen and helium during the long term anneal.

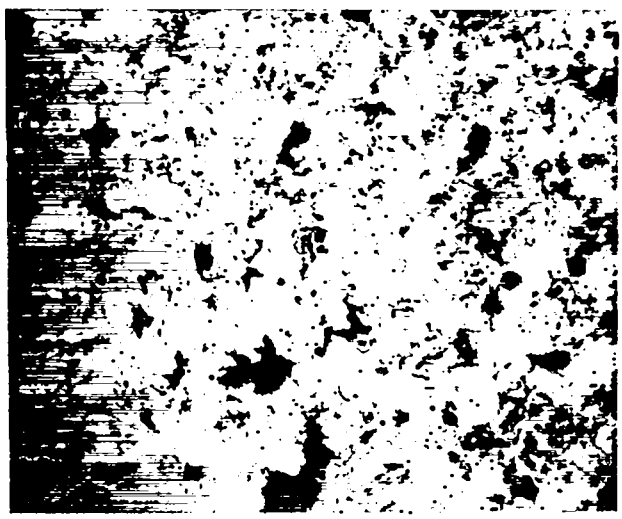

|200 μ|

Fig. 13. Typical $^{238}PuO_2$ Microstructure After Heating for 1000 h at 1800°C. Unetched.

Because of the persistent concern over welds in TZM, the HP-1 capsule closure weld was examined metallographically. This weld was found to be sound and appeared to be unaffected by the 1000 h, 1800°C heat treatment (see Fig. 14). The grains are indeed large in the weld area, but from experience they appear to be not much larger than those found in unheated TIG welds.

|200 μ|

Fig. 14. TIG Weld in TZM Capsule HP-1 after Heating for 1000 h at 1800°C. Etched with $K_3Fe(CN)_6$.

Capsule HPT-1, $^{238}PuO_2$-ThO_2 @ 1800°C.

Specimen HPT-1 was designed to test the compatibility of $^{238}PuO_2$-53 w/o ThO_2 with TZM at 1800°C. Its makeup and treatment were the same as described above for HP-1, except that $^{238}PuO_2$-ThO_2 solid solution pellets instead of 100% $^{238}PuO_2$ were used.

A photomicrograph of the fuel-TZM interface is presented in Fig. 15 and indicates that no reaction has resulted from the heat treatment. There is just a suggestion of a reaction layer in the TZM, but hardness measurements and previous experience indicate that this is simply a very fine-grained surface layer of otherwise unaffected TZM. Replica electron microscopy, which is presently underway, is expected to verify the fine-grained nature of this layer. The hardness trace seen in Fig. 16 reveals no change in properties through and adjacent to this region. The average hardness of the TZM measured both within 25 μm of the surface and at the center of the specimen was 223 VHN, which is not unusual for TZM. Precipitates are seen in this TZM specimen which are like those seen in TZM heated under similar circimstances (compare Figs. 12 and 16). The average hardness of the $^{238}PuO_2$-53 w/o ThO_2 solid solution was found to be 1267 VHN, which is significantly harder than the 100% $^{238}PuO_2$ in HP-1.

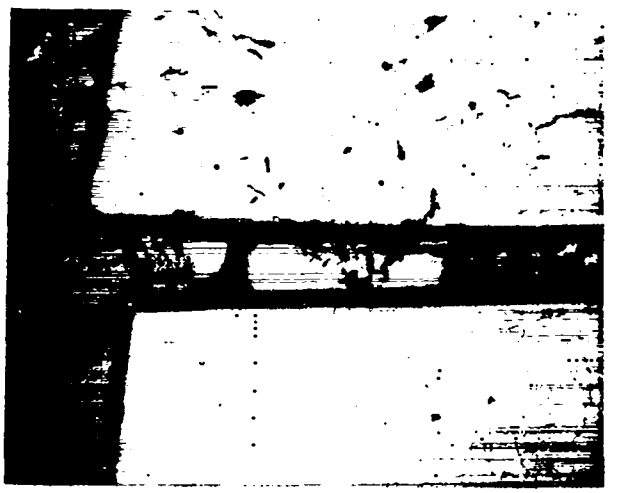

Fig. 15. TZM/$^{238}PuO_2$-53 w/o ThO_2 Interface after 1000 h at 1800°C. TZM Etched with $K_3Fe(CN)_6$.

Significant porosity was found in the $^{238}PuO_2$-53 w/o ThO_2 pellet after it had been heat treated (see Fig. 15), but the porosity does not appear to have segregated to the grain boundaries to the extent that it did in the 100% $^{238}PuO_2$. In contrast to the observation for $^{238}PuO_2$ (HP-1), whole grains did not appear to have been removed from

Fig. 16. Cross-section of the TZM Surface Held in Contact with $^{238}PuO_2$-53 w/o ThO_2 for 1000 h at 1800°C. $K_3Fe(CN)_6$ Etch.

the surface of the $^{238}PuO_2$-ThO_2 solid solution during the metallographic polishing.

Capsule D, $^{238}PuO_2$-ZrO_2 @ 900°C.

Compatibility specimen D was a duplicate of specimen C, which had been opened and examined earlier after 935 h at 900°C. Capsule D, however, was held for 6671 h at that temperature.

Both capsules contained pellets stacked to give the interfacial arrangement: $ZrO_2|Y|$/TZM/$^{238}PuO_2$-35 w/o $ZrO_2|Y|$/TZM/$^{238}PuO_2$-7 w/o $ZrO_2|Y|$. The pellets were stacked in a molybdenum foil sleeve which, in turn, was slipped inside an Inconel 718 tube. The tube was closed by TIG welding under ~1 in. Hg pressure of helium and was then sealed inside a second, larger Inconel 718 tube. This capsule assembly was heated in a vertical position which allowed a small TZM weight on top of the pellet stack to provide some additional interfacial pressure. A molybdenum hold-down spring helped to hold the TZM weight and the pellets in place.

The capsule was prepared for examination in much the same fashion as described above for HP-1. The TZM/$^{238}PuO_2$-7 w/o $ZrO_2|Y|$ interface (see Fig. 17)

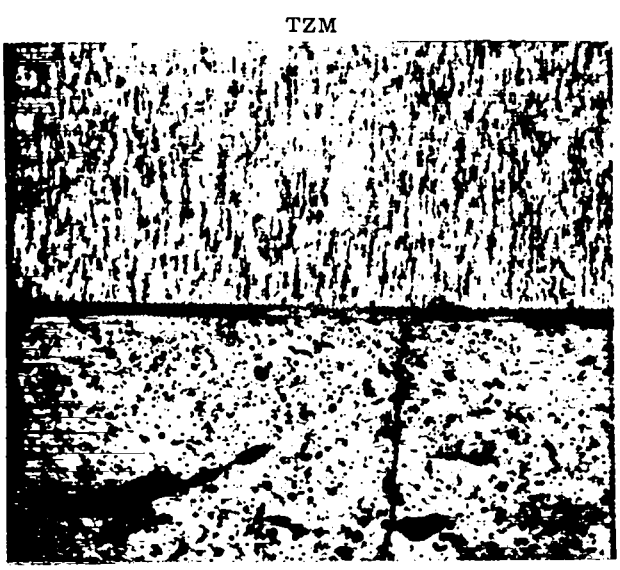

Fig. 17. TZM/$^{238}PuO_2$-7 w/o $ZrO_2|Y|$ Interface After 6671 h at 900°C. TZM Etched with $K_3Fe(CN)_6$.

showed no evidence of reaction, and, as shown in Fig. 18,

Fig. 18. Cross-section of TZM Surface Held in Contact with $^{238}PuO_2$-7 w/o $ZrO_2|Y|$ for 6671 h at 900°C. $K_3Fe(CN)_6$ Etch.

no change in the properties of the TZM were detected by hardness measurements started at a depth of 25 μm below the surface of the specimen. The average hardness of this TZM pellet was found to be 286 VHN, which is somewhat harder than was the TZM from the two compatibility specimens discussed above. This difference apparently lies in the fact that the 900°C heat treatment, even as long as it was, did not recrystallize the TZM.

The $ZrO_2|Y|$/TZM and $^{238}PuO_2$-35 w/o $ZrO_2|Y|$/TZM interfaces are shown in Figs. 19 and 20. No reaction layers were detected. For both TZM pieces, the hardness traverses at right angles to the interfaces showed no evidence of a hardened case. The average hardness of the TZM that had contacted the $ZrO_2|Y|$ was 289 VHN, and the hardness of the TZM that had contacted the $^{238}PuO_2$-35 w/o $ZrO_2|Y|$ was 306 VHN. Hardness measurements of 1480 and 1478 VHN, respectively, were obtained for the $^{238}PuO_2$-35 w/o $ZrO_2|Y|$ and $^{238}PuO_2$-7 w/o $ZrO_2|Y|$ pellets.

Capsule LP-4, $^{238}PuO_2$-ThO_2 @ 900°C.

The interfacial arrangement in LP-4 was: ThO_2/TZM/$^{238}PuO_2$-56 w/o ThO_2/TZM/$^{238}PuO_2$/TZM. This capsule was made up in the same manner as Capsule D, except that the capsule material for LP-4 was nickel-200. During final disassembly, the contents of the capsule were accidentally spilled, and the TZM pieces were

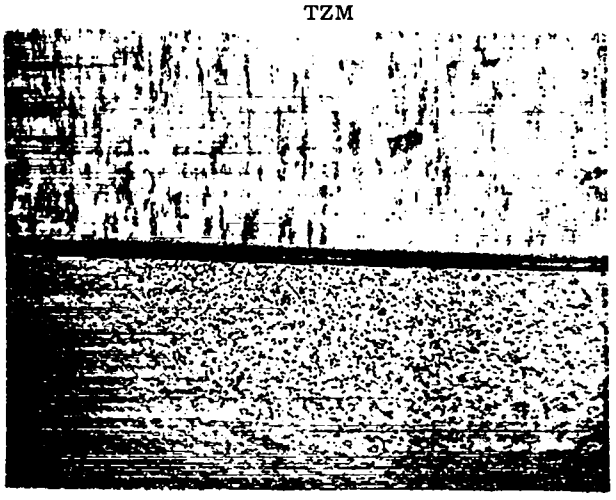

Fig. 19. TZM/$ZrO_2|Y|$ Interface after 6671 h at 900°C. TZM Etched with $K_3Fe(CN)_6$.

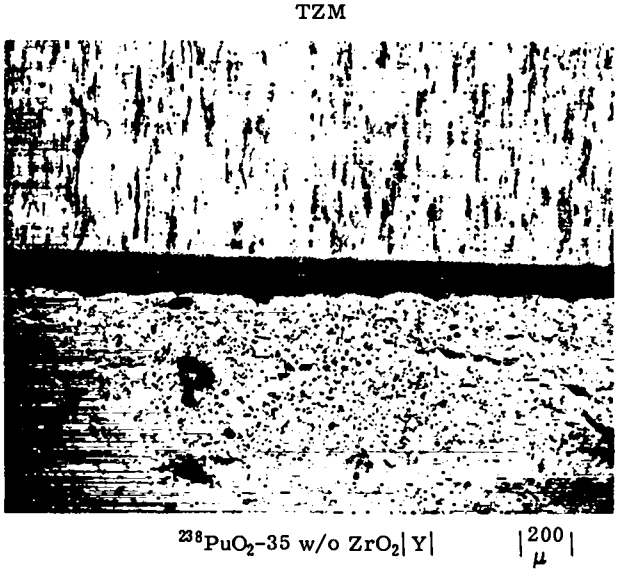

Fig. 20. TZM/$^{238}PuO_2$-35 w/o $ZrO_2|Y|$ after 6671 h at 900°C. TZM Etched with $K_3Fe(CN)_6$.

mixed up. Nevertheless, the three TZM pellets were mounted and examined metallographically. All three showed no sign of solid-solid reactions, but two showed some indication of a gas-solid reaction. That is, a reaction layer was seen which was continuous around the periphery of the specimen (see Fig. 21). The average hardness of this piece was 281 VHN, with no appreciable variation in hardness from surface to center. The layer was too thin to allow its hardness

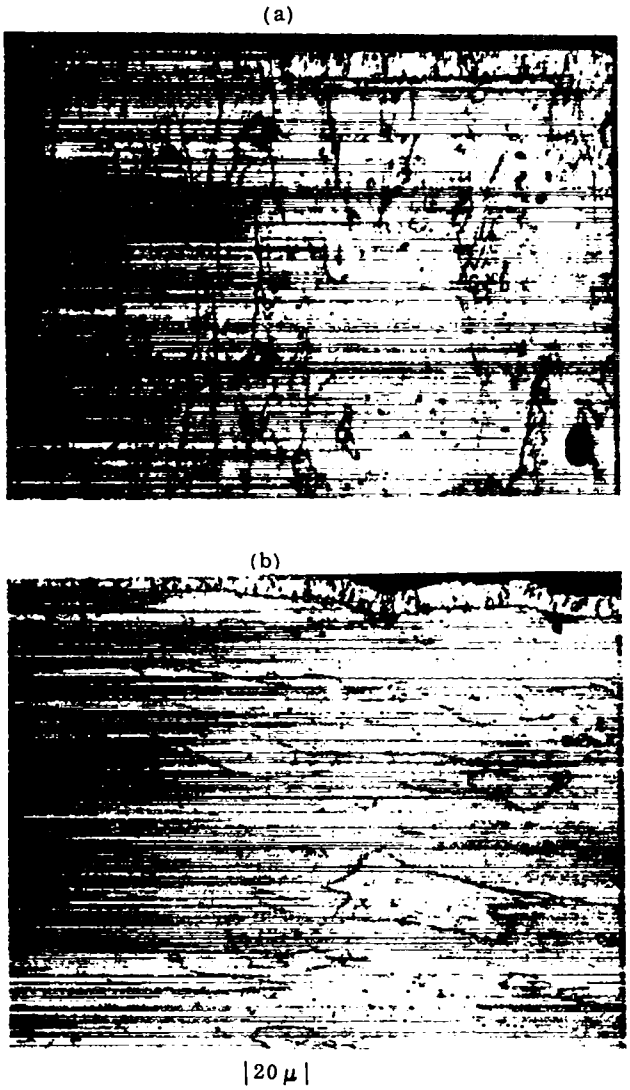

Fig. 21. TZM from Capsule LP-4 after 4910 h at 900°C.
(a) Edge near ceramic
(b) Outside diameter of pellet adjacent to Mo-foil liner.

to be measured. (L. B. Lundberg and R. E. Tate)

B. Impact Testing:

The results of the determination of the post-impact, particle-size distribution in sample BMI AA-61 indicate that a maximum fraction of 0.0015 of the initial sample was present as particles smaller than 10μm.

BMI sample AA-61 was impacted at Mound Laboratories on September 22, 1969. The velocity at impact was 248 fps, and the temperature was estimated to be 50°C. The sample was doubly contained, the inner container being a closely fitting, welded, stainless

steel capsule, and the outer being a thick-walled impact capsule. The impact capsule was closed by means of a copper-gasketed screw cap and a welded cap.

After being impacted, the capsule was shipped to LASL where it was opened. The welded cap was removed by machining, and the inner cap was unscrewed, with some difficulty, under the surface of liquid CCl_4. The inner capsule was found to be deformed, as was the thick-walled impact capsule, and broken in the region of the bottom weld. The fracture was relatively small.

The instructions for opening the capsule called for grinding off the welded lip of the inner capsule, removing the cap and, presumably, shaking out the sample. However, the deformation of the inner capsule, combined with the sizes of the broken pieces of the sample, prevented all but a small portion of the fuel from being recovered in this manner. It was found necessary to grind off the bottom of the inner capsule, too. Periodically, during both grinding processes, the inner capsule and the sample it contained were immersed in CCl_4. Some of the fuel particles were recovered in this way, but some of the stainless steel grinding residue was also entrained in the CCl_4. Presumably, some alloying of the PuO_2 with the stainless steel had occurred during welding, because a light-blue, flocculent precipitate formed in the CCl_4.

The recovered fuel, with the exception of that entrapped with the grinding residue, was wet sieved under CCl_4 and ultrasonic agitation. To recover that portion of the fuel combined with the grinding residue, the CCl_4 was evaporated and water added. The precipitate persisted until the acidic liquid was made basic by the addition of NaOH, and a clear, yellow-brown liquid formed over dark particles, presumably of both PuO_2/Mo and stainless steel. This liquid was decanted and the particles washed. Then the stainless steel was dissolved in a mixture of 3 parts nitric and 2 parts acetic acids, and the PuO_2/Mo was recovered and analyzed for particle size.

The distribution of the particles present after impact is given in Table IV.

In Table V, the fraction of fines < 10μm produced in this impact test may be compared to the corresponding fractions obtained in two other impact tests examined at LASL. (S. E. Bronisz and R. E. Tate)

Table IV

POST-IMPACT PARTICLE SIZE FRACTIONS
Sample: BMI-AA-61

Size, μm	Weight, g	Fraction of Initial Weight	Accumulated Fraction
Piece No. 1*	5.6939	0.3678	0.3678
Piece No. 2*	5.1865	0.3350	0.7028
Piece No. 3*	3.4774	0.2246	0.9274
> 841	0.8024	0.0518	0.9792
> 420	0.0782	0.0051	0.9843
> 177	0.0302	0.0020	0.9863
> 125	0.0155	0.0010	0.9873
> 74	0.0292	0.0019	0.9892
> 44	0.0204	0.0013	0.9905
> 30	0.0274	0.0018	0.9923
> 20	0.0329	0.0021	0.9944
> 10	0.0657	0.0042	0.9986
< 10	0.0234	0.0015	1.0001
Recovered Weight	15.4831 g		
Initial Weight	15.4686 g		
Excess	0.0145 g		

*The three large pieces were weighed separately.

C. Advanced Isotopic Heat Source Fuels:

The possibility of using ^{238}Pu, in some form other than the oxide, as the fuel material for isotopic heat sources has received some attention. A review of the published phase diagrams of plutonium revealed that the compound $PuPt_2$ had much to recommend it for this use. It is stable as a single phase over a 2 a/o compositional range (66 to 68 a/o Pt), making it relatively easy to establish production specifications. Its melting point, ~1475°C, is not too high for easy fabrication, it could be cast, nor too low for high-temperature capability. Its use would eliminate the problems associated with α-n reactions in PuO_2. Assuming 80% ^{238}Pu, its theoretical power density would be 3.2 watts/cc, thermal.

A test alloy made to the composition $PuPt_2$ was arc cast and held in vacuum at 900°C for one month. After the heat treatment, the sample was broken in a vise. One piece was polished metallographically and examined. The material proved to be so resistant to chemical attack that it could not be etched by any of the usual methods, and thus, all microscopic examinations

Table V

FINES PRODUCTION IN THREE IMPACT TESTS

Sample No., Description	Impact Velocity, fps	Fraction < 10μm
BMI-AA-61, $^{238}PuO_2$/Mo, contained	248	0.0015
7-114-1A, $^{239}PuO_2$ ceramic, uncontained	127	0.0062
AI-T8-3, ThO_2/Mo full scale	386	0.0067

were carried out on as-polished surfaces.

The microstructure consisted of relatively equiaxed grains of $PuPt_2$ (hardness 902 DPHN), partially outlined by grain boundary precipitates, as shown in Fig. 22.

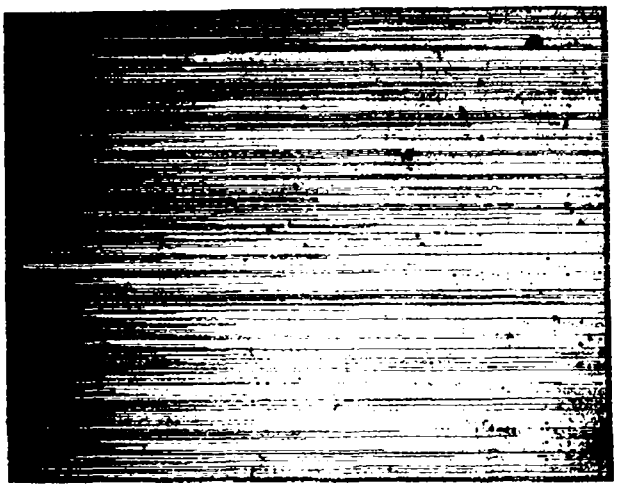

|20μ|

Fig. 22. Microstructure of $PuPt_2$ that had been Arc Cast and Heat Treated in Vacuum for 1 Month at 900°C.

The amount of grain boundary material was somewhat greater near the surface of the sample, but the difference was relatively minor, since the measured density of the sample was 18.5 g/cc compared with the theoretical density of 18.69 g/cc.

After two weeks exposure to laboratory air, the fracture surfaces were as clean and untarnished as when they were fresh. One piece of the sample was held for five minutes at 900°C in air. The extent of reaction is shown in Fig. 23. The reaction zone consists of four layers, five phases, with a combined thickness of 60-80μm. It is interesting to note that in those areas where grain boundary penetration is evident, the innermost layer is either very thin or missing entirely. The sample contained several cracks near its surface after the heat treatment in air. Since the reaction zone was on the surfaces of the cracks as well as on the original surfaces, the indication is that the cracks were probably formed when the sample was heated. The reaction zones in both areas are shown in Fig. 24. Fig. 25 shows that both the outer and inner layers were optically active.

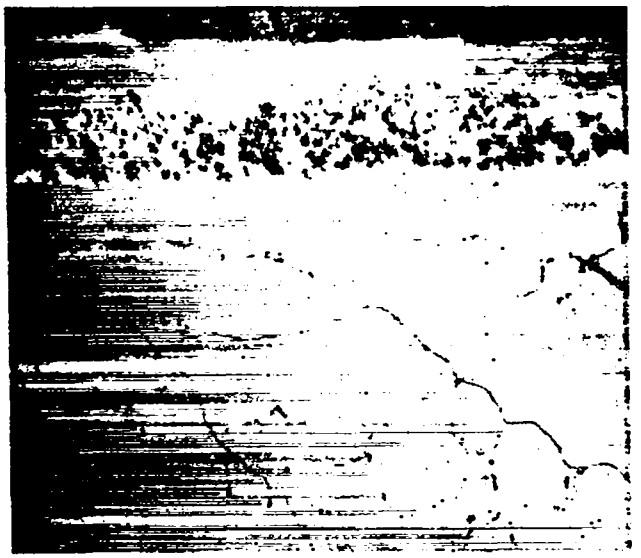

|20μ|

Fig. 23. Reaction Zone on Original $PuPt_2$ Surface.

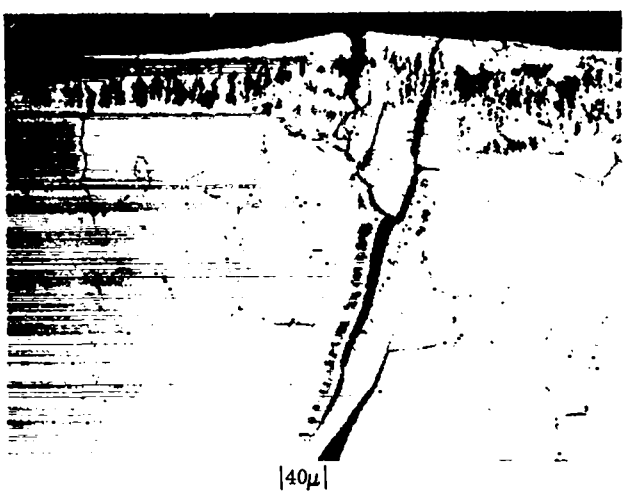

|40μ|

Fig. 24. Reaction Zones on $PuPt_2$ Surface and Along Crack.

Electron microprobe analysis of the grain boundary precipitates indicated the presence of less platinum and more plutonium than in the matrix grains and suggests that the precipitates are the adjacent compound PuPt.

The fracture surface on the third piece of the sample was replicated for examination by electron microscopy and was also examined directly in the Scanning Electron Microscope. Nearly all of the fracture surface was of the cleavage type, indicating brittle behavior at room

|40μ|

Fig. 25. Same as Fig. 14, Except Polarized Light.

temperature. One small area of ductile fracture in a porous region near the surface of the sample was found with the scanning microscope. (S. E. Bronisz and R. E. Tate)

D. Interdiffusion of Refractory Metals:

It is of engineering interest to predict the long term interdiffusion behavior of the refractory metals Nb, Mo, Ta, and W, which might be used in a variety of combinations for structural applications in the 800 to 1400°C [1500 to 2500°F] temperature range. These elements all have body-centered cubic structures, and examination of the phase diagram compilations of Hansen,[1] Elliott,[2] and Shunk[3] indicates complete mutual solid solubility between all possible binary combinations of the four elements. There is fragmentary evidence for an intermetallic compound in both the W-Nb and M-Mo systems (a feature which would modify diffusion behavior), but there is equally good evidence for lack of compounds.

The most comprehensive sources of diffusion data are the book of Adda and Philibert[4] published in 1966 and the recently started journal "Diffusion Data".[5] Very little data in the temperature range of interest are available in the literature, probably because the relatively slow interdiffusion rates (the very feature which creates engineering interest) require long term diffusion experiments. The available data and the original references are given in Table VI.

Perhaps a better way to present the data is in the form of conventional log D vs 1/T plots. Figures 26 through 29 show the available data; each figure considers the elements Nb, Mo, Ta, and W in turn as the matrix. The temperatures of interest, 1500, 2000, and 2500°F, are also plotted. Perusal of these figures shows that, though the data are in general agreement, most of the data points lie outside the temperature range of immediate interest and the calculations involve considerable extrapolation. At temperatures below half the absolute melting point, plotted as MP/2 for each matrix element, short circuiting paths such as grain-boundary diffusion become significant, and diffusion is likely to proceed appreciably faster than a linear extrapolation of log D vs 1/T would indicate.

Educated guesses suggest that the interdiffusion coefficients of interest lie in the range of 10^{-15} to 10^{-11} cm^2/sec. Values of penetration in mils have been calculated using the appropriate diffusion equation for diffusion coefficients in this range and for times of 1 day

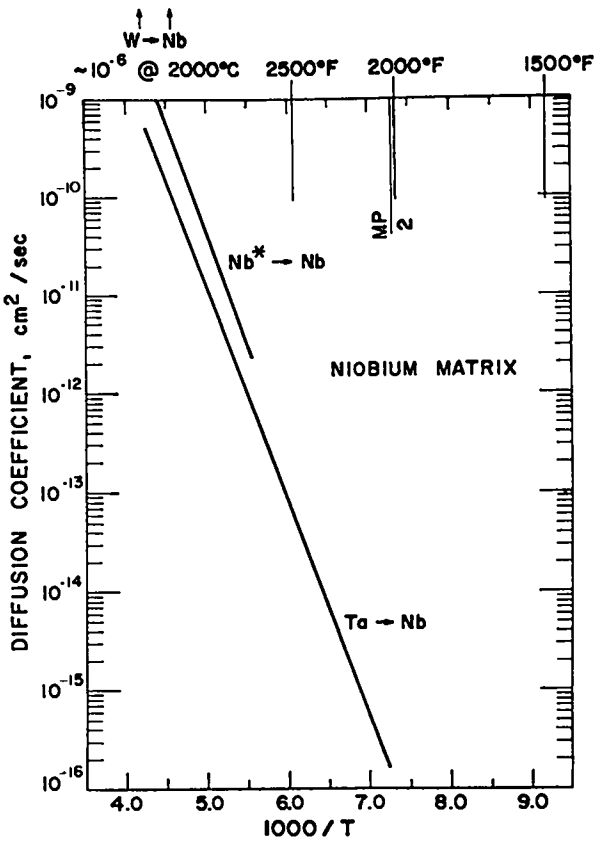

Fig. 26. Log D vs. 1/T for Niobium Matrix.

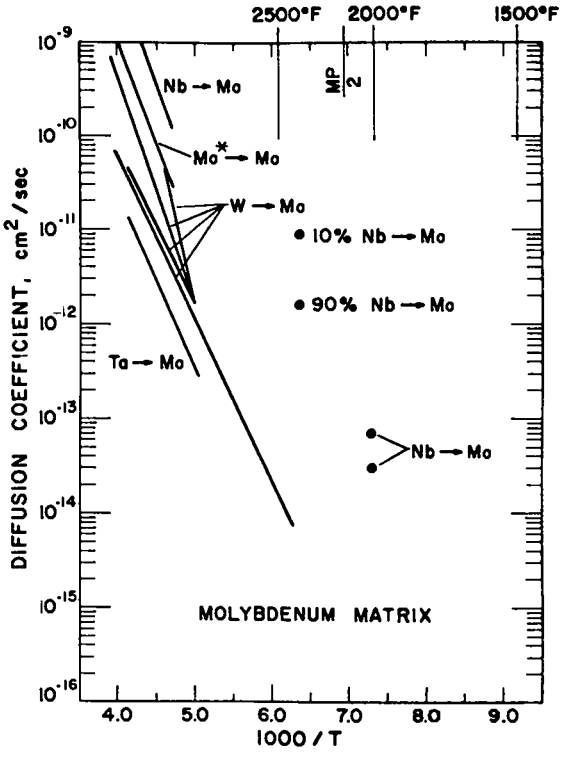

Fig. 27. Log D vs 1/T for Molybdenum Matrix.

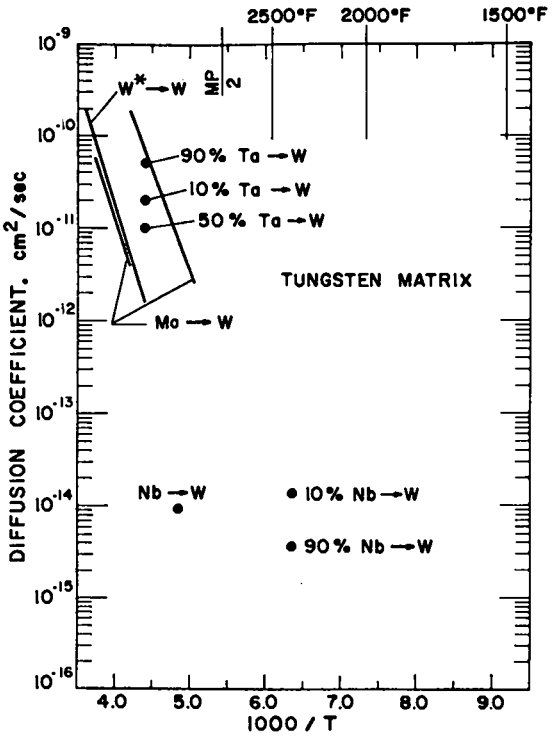

Fig. 29. Log D vs 1/T for Tungsten Matrix.

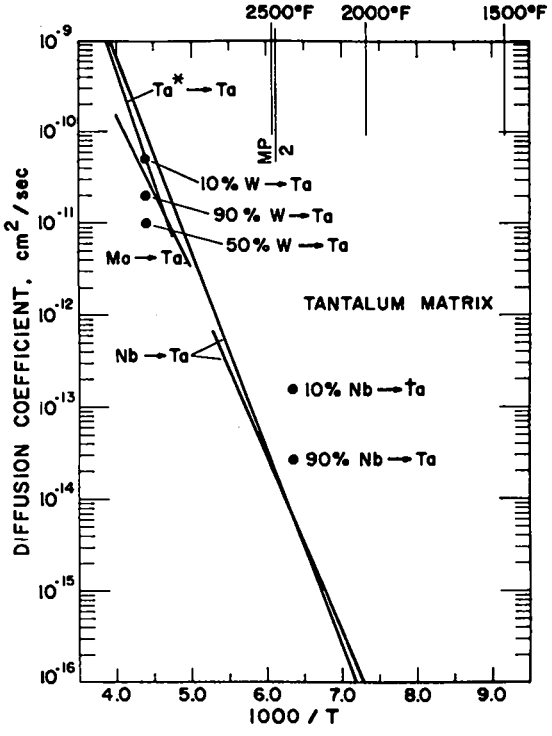

Fig. 28. Log D vs 1/T for Tantalum Matrix.

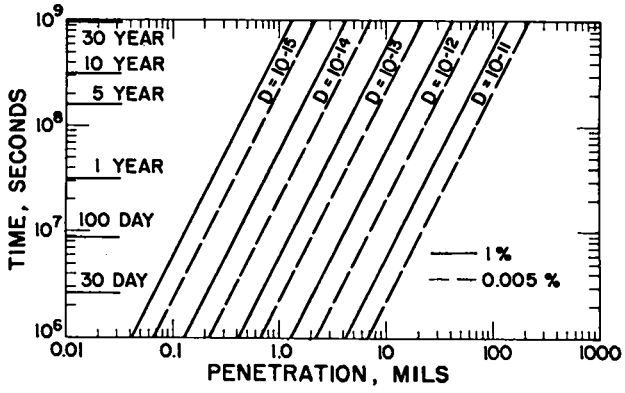

Fig. 30. Penetration Plot.

Table VI

SUMMARY OF DIFFUSION DATA FOR Nb, Mo, Ta, AND W BINARY COMBINATIONS

	Type of Data	Experimental Temperature, °C	D_o cm^2/sec	Q kcal/mole	C At.%	D cm^2/sec	Ref.
Nb* → Nb	Self	1535 - 2120	12.4	105			6
Ta → Nb	Tracer	1103 - 2073	1	99.3			7
W → Nb	Inter	1900			10 W	1.16×10^{-7}	8
	Inter	1900			90 W	5×10^{-9}	8
	Inter	2100			10 W	1.4×10^{-5}	8
	Inter	2100			90 W	1.6×10^{-7}	8
Mo* → Mo	Self	1850 - 2350	0.1	92.2			9
Nb → Mo	Tracer	1850 - 2350	14	108.1			10
	Inter	1100				3 to 7×10^{-14}	11
	Inter	1300			10 Nb	8.75×10^{-12}	12
	Inter	1300			90 Nb	1.67×10^{-12}	12
Ta → Mo	Tracer	1700 - 2150	3.5×10^{-4}	83			23
W → Mo	Inter	1400 - 2260	6.3×10^{-4}				13
	Tracer	1700 - 2260	1.7	110			14
	Tracer	1700 - 1900	3.18	112.9			15
	Tracer	1700 - 2150	4.5×10^{-4}	77.5			23
Ta* → Ta	Self	1827 - 2527	2	110			16
Nb → Ta	Tracer	1050 - 1600	0.02	90			17
	Tracer	920 - 2500	0.23	98.7			18
	Inter	1300			10 Nb	1.58×10^{-13}	12
	Inter	1300			90 Nb	2.76×10^{-14}	12
Mo → Ta	Tracer	1750 - 2220	1.8×10^{-3}	81			23
W → Ta	Inter	2000			10 W	5×10^{-11}	19
	Inter	2000			90 W	2×10^{-11}	19
W* → W	Self	2000 - 2700	0.54	120.5			20
Nb → W	Inter	1300			10 Nb	1.39×10^{-14}	12
	Inter	1300			90 Nb	3.75×10^{-14}	12
	Inter	1800				8.95 to 9.85×10^{-15}	21
Mo → W	Tracer	2100 - 2400	3.7×10^{-3}	110			22
	Tracer	1700 - 2100	0.3	101			23
Ta → W	Inter	See W → Ta					19

to 10 years. The results of this computation are presented numerically in Table VII and graphically in Fig. 30. An important assumption in the mathematics is that the diffusion coefficient is independent of concentration, an assumption that must be made in the absence of actual data. The real situation is likely to be that shown in Fig. 31 (D vs % for W-Ta at 2000°C), where it can be seen that D varies by a factor of five across the composition range.

The figures presented were designed to estimate penetration in the following way:

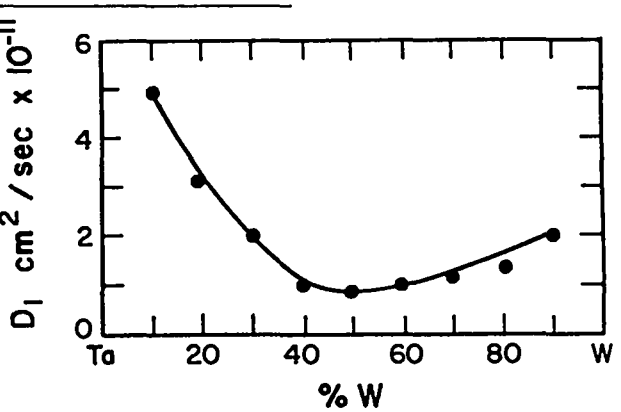

Fig. 31. The Chemical Diffusion Coefficient in the System W-Ta at 2000°C as a Function of Composition.[19]

Table VII

CALCULATED DISTANCE FROM INTERFACE WHERE SOLUTE CONCENTRATION IS 1% AND 0.005%

D cm^2/sec	Solute Concentration (%)	1 day 8.64×10^4 sec	100 days 8.64×10^6 sec	1 yr - 365 d. 3.1536×10^7	5 years 1.5768×10^8	10 years 3.1536×10^8
10^{-11}	1	1.2	12.0	23.1	51.6	72.8
	0.005%	2.0	20.1	38.5	85.8	122
10^{-12}	1	0.38	3.81	7.28	16.3	23.1
	0.005%	0.64	6.38	12.2	27.3	38.5
10^{-13}	1	0.12	1.20	2.31	5.16	7.28
	0.005%	0.20	2.01	3.85	8.58	12.2
10^{-14}	1	0.04	0.38	0.73	1.63	2.31
	0.005%	0.06	0.64	1.22	2.73	3.85
10^{-15}	1	0.01	0.12	0.23	0.52	0.73
	0.005%	0.02	0.20	0.38	0.86	1.22

Penetration in mils

1) Select a diffusion coefficient at the desired temperature from the appropriate matrix plot. Keep in mind that the diffusion coefficient is almost certain to be larger (smaller exponent) than a linear extrapolation suggests.

2) Refer to Table VII or Fig. 30 and read a penetration in mils for an appropriate time, using the row or line corresponding to the diffusion coefficient estimated in Step 1. Note that it is possible to select a penetration corresponding to a concentration level of 1% or 0.005% of the solute. Keep in mind the approximate nature of the calculated penetration due mainly to the extrapolation to lower temperature and to the probable variation of the diffusion coefficient with concentration. (R. E. Tate)

E. Miscellaneous Properties

Various investigations, tests, and studies have been in progress as part of Tasks V.2 and VI.1. Results and status of these studies are given in the following sections.

1. Product Chemistry (V.2)

Typical composition of both coated and uncoated SSC specimens along with quantitative analytical results are given in Table VIII.

Table VIII

THEORETICAL AND DETERMINED COMPOSITION OF SSC MATERIAL

Element	w/o Theoretical Coated	w/o Theoretical Uncoated	w/o Determined Uncoated Specimens 1	w/o Determined Uncoated Specimens 2
Pu	66.1	68.8	68.8	68.6
Th	7.3	7.6	7.9	8.2
Mo	16.6	13.3	13.8	12.7
O	10.0	10.3	....	10.0
U	....	....	0.48	0.08

Note: ^{234}U grows in at rate of 525 ppm per month
^{237}Np concentration is variable.

2. Microstructure

A microstructure of a representative SSC specimen is shown in Fig. 32.

3. Emission Spectroscopy

Results of an emission spectrographic analysis of two typical SSC specimens are shown in Table IX. The values for Ta reflect the use of a Ta liner in these pressings. This contaminant at these levels has not been observed in later analysis since this die liner material is no longer employed. The limits shown in Table IX (see next page) are limits of detection.

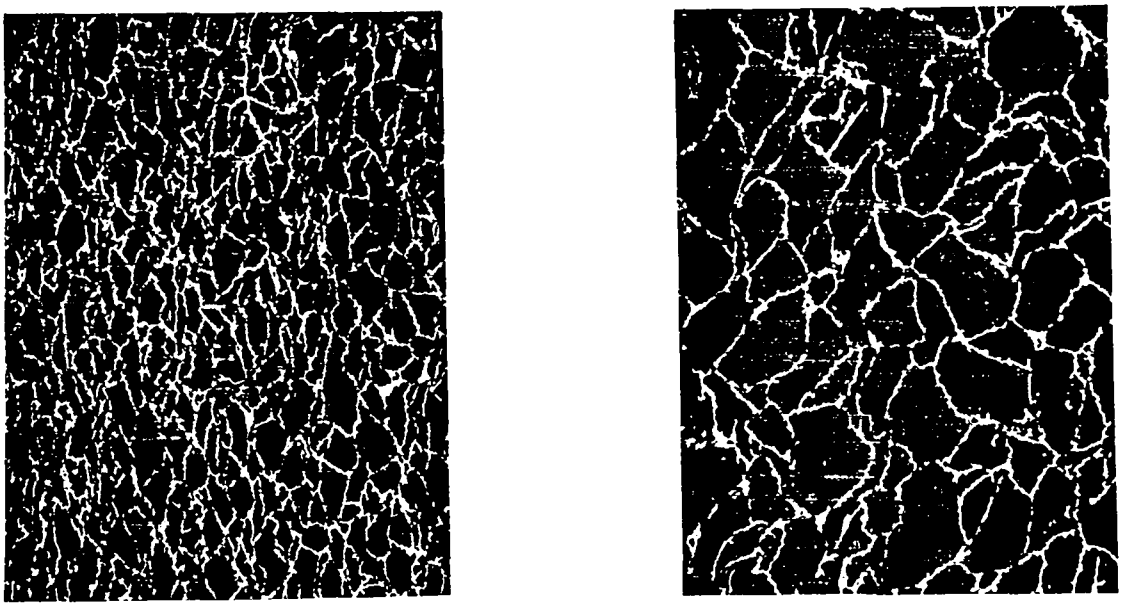

| 200 μ | | | 200 μ |

Fig. 32. Microstructure of Representative SSC Specimen

Table IX

EMISSION SPECTROSCOPIC ANALYSIS OF TYPICAL SSC SPECIMENS

Element	Specimen No. 1, ppm	Specimen No. 2, ppm
Be	< 1	< 1
B	< 2	< 2
Na	< 50	< 50
Mg	2	4
Al	< 10	700 est.
Si	10	130
Ca	20	700 est.
V	< 4	< 4
Cr	< 20	20
Mn	2	< 2
Fe	30	170
Ni	10	< 5
Cu	20	10
Zn	< 20	< 20
Sr	< 5	< 5
Zr	< 1000	< 1000
Nb	400	800
Cd	< 5	< 5
Sn	< 5	< 5
Ta	2000 est.	800
Pb	< 5	< 5
Bi	< 1	< 1

4. Thermal Stability of Uncoated SSC in Air (VI. 1.3)

The following results were observed upon heating an uncoated specimen in air under the stated conditions.

Table X

OBSERVED CHANGES AFTER HEATING UNCOATED SSC SPECIMEN IN AIR

Temp., °C	Time, hr.	Observation
100	24	No change
200	24	No change
300	24	No change
400	24	0.6 w/o gain; some tarnishing
500	24	Power formation

5. Vaporization of Uncoated Specimen and Examination of Emitted Species by Mass Spectrographic Techniques (VI. 1. 12)

The following observations and conclusions resulated from vacuum heat treatment of an uncoated SSC specimen in a mass spectrograph. Analogous studies on a coated specimen are in progress. Results will be presented in the next quarterly report.

MASS SPECTROGRAPHIC (VACUUM) EXAMINATION OF UNCOATED SSC SPECIMEN
(Not previously outgassed)

A.) Low-Temperature (< 825°C) Heating

1) At ≤ 200°C, He pressure was 2.5×10^{-4} atm. HF was barely detected at < 10^{-8} atm. He was released smoothly as the temperature was increased to 800°C.

B.) High-Temperature (> 825°C) Heating

1) From 800-900°C, some Pu and Mo fluorides were observed. These were released smoothly and by 1400°C, no fluorides were detected.

The following table gives pressure data for MoF_6 and PuF_3.

Table XI

VAPOR SPECIES AND PRESSURES

T, °C	MoF_6, atm	PuF_3, atm	He, atm
1050	1.9×10^{-5}	4.1×10^{-8}	3.2×10^{-6}
1086	1.4×10^{-5}	7.7×10^{-8}	3.2×10^{-6}
1200	1.1×10^{-6}	5.2×10^{-8}	1.9×10^{-6}
1227	7.6×10^{-7}	6.2×10^{-8}	1.6×10^{-6}

2) At ~1500°C, PuO_2 appeared. A Ta crucible was used in this experiment and $PuO_2(g)$ would be reduced in this environment. The next table gives pressure data for this species as a function of temperature.

Table XII

PuO_2 PRESSURES vs. TEMPERATURE

T, °C	PuO Pressure, atm, $\times 10^7$
1600	1.7
1663	5.2
1686	7.6

C.) Conclusions on Non-Outgassed Specimens

1) He and barely detectable HF are released smoothiy at ≤ 300°C.

2) Some MoF_6, PuF_3, and additional He are released over the range 800-1400°C. Overall pressures are very low.

3) PuO appears at 1500°C.

6. Differential Thermal Analysis (DTA) of Coated SSC Specimen (VI. 1. 16)

A coated specimen was heated in the DTA apparatus to 2100°C under 0.5 atm argon. The specimen was then cooled and a portion broken off for metallographic examination. The remaining portion of the specimen was reheated.

No thermal arrests were observed below 2450°C. Visual examination of the specimen up to 2425°C indicated no evidence of slumping, edge rounding, or other macro evidence indication of liquidus formation. Solidus phases persisted at 2450 ± 25°C. Liquidus formation beginning above this temperature gave a gradual lag on the DTA tracings which is indicative of multiple processes. Melting was complete by 2665°C.

7. Thermal Expansion (VI. 1. 22)

Eight coated SSC specimens were used to determine the following thermal expansion data.

Table XIII

THERMAL EXPANSION OF COATED SSC

Temp., °C	Percent Expansion $(\Delta L/L_o)$ (100)
100	0
200	0.053
300	0.11
400	0.17
500	0.24
600	0.30
700	0.37
800	0.43
900	0.49

Avg. Thermal Expansion from 100°: 6.2×10^{-6} in./in./°C

8. Spectral Thermal Emittance of Coated SSC Specimen (VI. 1. 25)

The normal spectral thermal emittance of a coated SSC specimen was measured over the range 797-1445°C. The specimen had three cavities drilled before overcoating with Mo. Dimensions of these cavities are: (1) 0.021 in. dia x 0.022 in. deep; (2) 0.031 in. dia x 0.027 in. deep; and (3) 0.051 in. dia x 0.050 in. deep. The specimen was heated inductively in a Mo metal cylinder.

Over the stated temperature range, 55 sets of measurements were made of the cavity and the surface temperatures of the specimen and 16 corresponding measurement sets were made on the Mo holding cylinder. Emittances were calculated from the equation:

$$\ln (E_s/E_c) = (C_2/\lambda)\,(1/T_c - 1/T_s)$$

where E_s = surface emittance

E_c = cavity emittance

T_s = apparent surface temperature

T_c = apparent cavity temperature

C_2 = 1.4388 cm (radiation constant)

λ = 0.65 μ (wavelength)

Using appropriate assumptions of diffuse reflectance from the cavity walls, the normal spectral thermal emittance of the specimen was calculated to be 0.76 ± 0.05 at the stated wavelength.

9. Radiation Characteristics of SSC (VI.1.26)

Studies have demonstrated the feasibility of removing fluoride contaminant from SSC which in turn decreases the neutron emission rate due to the (α, n) reaction on fluorine. Some fluorine contaminant resulting from the decomposition of MoF_6 is unavoidable. The purpose of the current investigation was to decrease this contaminant to a tolerable level for the TRANSIT application.

A vacuum bake-out of coated feed powder and finished specimen was effective in reducing the overall neutron emission. The following information was obtained as a result of feed powder vacuum equilibration.

Table XIV

NEUTRON EMISSION FROM $^{238}PuO_2$-ThO_2 POWDER

Material	n/sec/g Pu	Treatment
"As Milled"	17,600	After milling and blending
Coated Powder	59,840	After CVD coating; obviously contains fluorine
Coated Powder	34,110	1600°C for 2 hr in vacuum
Coated Powder	21,070	1800°C for 2 hr in vacuum

Analagous treatment was given to a finished pellet with the following results.

Table XV

NEUTRON EMISSION FROM SSC SPECIMEN

Material	n/sec/g Pu	Treatment
"As Received" SR Oxide	13,900	None
SSC Specimen	33,880	"As fabricated" (No outgassing of feed powder)
SSC Specimen	30,190	1400° for 2 hr in vacuum
SSC Specimen	21,070	1600° for 2 hr in vacuum

Table XV, continued

Material	n/sec/g Pu	Treatment
SSC Specimen	18,030	1800° for 2 hr in vacuum

Final treatment of coated feed powder and finished disc will be done on all standard SSC discs.

IV. DESIGN AND INSTALLATION

A. 50-Ton Hot Press

Final fabrication, assembly, and installation of this unit in a ^{238}Pu enclosure was completed during this quarter. This unit is now fully operational.

B. Lorch Lathe

A Lorch Lathe was procured during this quarter. A ^{238}Pu enclosure for this lathe, the core-drilling device, and the jewelers' lathe was designed and fabricated. All of these machine tools are now operational on ^{238}Pu.

C. Ultrasonic Machine Tool and Facility

An ultrasonic machine tool was ordered and received during this quarter. Check-out of this tool in a cold area is in progress. The ^{238}Pu facility for this tool has been fabricated and is ready for installation.

D. Stand-by Barrel Coater

A stand-by barrel coater was fabricated and is ready for installation if needed.

V. HELIUM MIGRATION

A. Alpha-Particle Bombardment Effects in ThO_2

Annealing of Lattice Damage - In the previous quarterly report (see CMF-5 Quarterly Report, First Quarter FY 1970, SEPO/LASL Program 07433, ^{238}Pu Fuel Development, October 2, 1969) an experiment was described in which an attempt was made to determine the lattice parameter annealing curve of ThO_2 which had been bombarded with 5 MeV alpha particles to a dose of 1.9×10^{17} ions/cm^2. The experiment was terminated prematurely when the sample spalled after 1 h at 700°C.

Another ThO_2 sample, this one bombarded to 9.4×10^{16} ions/cm^2, is now under study in the same kind of experiment. To date, the sample has been heated in 1-hr annealing steps up to 1600°C, and the lattice parameter obtained at room temperature between anneals. The sample temperature during bombardment was about

160°C.

Results obtained are shown in Fig. 33, where data determined elsewhere in a similar experiment on PuO_2[24] are shown for comparison. It may be seen that recovery of lattice damage is a higher-temperature process in ThO_2 than in PuO_2, in agreement with the higher melting point of the former oxide. Although ~90% of the lattice dilation was removed after 1 hr at 1000°C, the remainder of the damage has proved quite resistant to further annealing and has not disappeared after 1 hr at 1600°C. PuO_2 did not show such resistance to annealing.

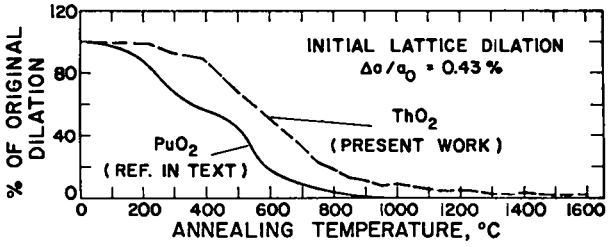

Fig. 33. Lattice Parameter Annealing Curve for Alpha-bombarded ThO_2.

The present ThO_2 sample spalled after 1 hr at 750°C, although fortunately not in the portion of the bombarded area being X-rayed. The spalling had the virtue of giving access to the area where alpha particles came to rest (~15μ penetration). After 1 hr at 1250°C, ThO_2 flakes were extracted from the spall region by replication techniques and examined by transmission electron microscopy. The results indicate that a large concentration of fine defects and dislocation loops is still present after such an anneal (Fig. 34).

Helium Bubble Formation - Also in the previous quarterly report (October 2, 1969), the discovery of helium bubbles in a flake of ThO_2 extracted from the spall region was described. Since this was an isolated observation, further search has been made for other bubbles. The results show that bubbles can generally be found at the helium deposition (spall) depth, although not in large numbers. Figure 35 shows bubbles in a sample bombarded to a dose of 3.8×10^{17} ions/cm^2. (F.W. Clinard, Jr.)

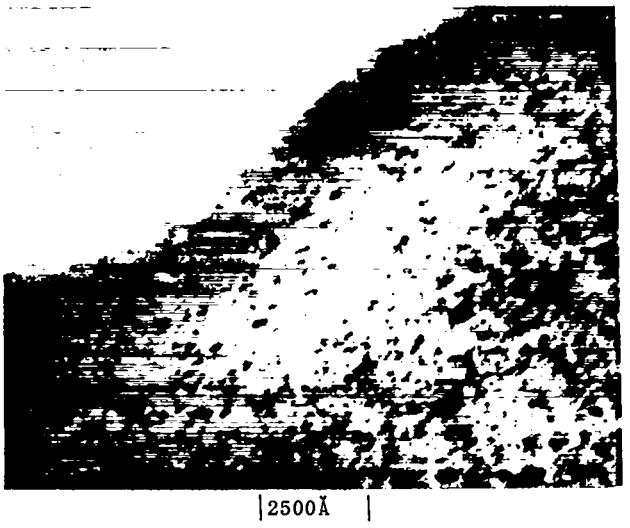

Fig. 34. Defect Structure of ThO_2 After Alpha-Particle Bombardment and Subsequent Annealing for 1 hr at 1250°C.

B. X-ray Diffraction

A disc of $^{238}PuO_2$ approximately 1/2" in diameter and 1/8" thick has been examined by X-ray diffraction techniques in the XRD-3 diffractometer for a period of 30 weeks at room temperature in an effort to measure any line broadening which, in turn, can be used to calculate crystallite size and strain in the lattice. The results, to be described and illustrated below, indicate that under the influence of self-irradiation the damage to the lattice is very small, in terms of small crystallite size and significant strain.

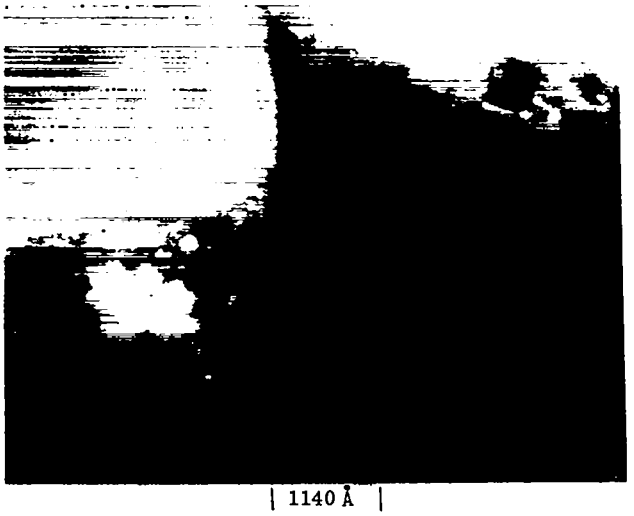

Fig. 35. Alpha-Bombarded ThO_2 After Being Beam Heated, Showing Helium Bubbles.

The most noticeable effect was the slight increase in the lattice constant of the material. See Table XVI.

Table XVI

LATTICE CONSTANT OF $^{238}PuO_2$ AS A FUNCTION OF TIME AFTER ANNEALING

Time, weeks	a_o, Å
4, 5, 6	5.41377 ± 34
7, 8, 9	5.41423 ± 36
10, 11, 12	5.41449 ± 38
13, 14, 15	5.41472 ± 42
16, 17, 18	5.41477 ± 49
19, 20, 21	5.41504 ± 50
22, 23, 24	5.41537 ± 45
25, 26, 27	5.41533 ± 66
28, 29, 30	5.41521 ± 49

Figure 36 illustrates the magnitude of the change. Least-squaring the data to the equation

$$y = a + bx + cx^2, \qquad (1)$$

where y = lattice constant and x = weeks after an initial anneal of the sample, we find

$a = 5.41309 \pm 15$
$b = 1.552 \pm 216 \times 10^{-4}$
$c = -2.752 \pm 650 \times 10^{-6}$.

The lattice constant was determined by processing the observed 2θ values of the reflections 111, 200, 220, 311, 333, 511, and 622 through LCREF, the Los Alamos lattice parameter refinement code, which provides the proper extrapolation function for diffractometer data. The observed 2θ values of the reflections were determined by least-squares fitting X-ray counts per second at specific 2θ values to the equation

$$y = A + Bx + Cx^2 + \ldots$$

$$\ldots + \sum_{j=2}^{\leq 13} \frac{D_{3j-2}}{\sqrt{2\pi} \cdot E_{3j-1}} \cdot e^{1/2\left(\frac{x-F_{3j}}{E_{3j-1}}\right)^2} \qquad (2)$$

which consists of a common background part and the sum of 13 or fewer Gaussian curves. A, B, C are the parameters for a polynominal background, D is the area under the Gaussian peak, E is the Gaussian half-width, F is the 2θ position of the peak, and y = counts per second at a specific x = 2θ position. In order to obtain a more reliable measure of the diffraction peak we find it convenient to average the data taken over a three week period. This seems reasonable since the effects we are interested in measuring occur quite slowly as a function of time. Thus, the points plotted in Fig. 36 are to be interpreted as having a horizontal spread of three weeks. Figure 37 illustrates the appearance of the 622 peak for the period of 7-9 weeks after the initial anneal. The resolution between $K_{\alpha 1}$ and $K_{\alpha 2}$ is quite good, indicating that strain is small and crystallite size is large.

In Eq. (2) the term $D_{3j-2}/\sqrt{2\pi} \cdot E_{3j-1}$ represents the height of the peak above background. Since D_{3j-2} is the area under the peak, the term $\sqrt{2\pi} \cdot E_{3j-1}$ is the integral breadth of the peak, and E_{3j-1} is, therefore, a direct measure of any broadening that may occur. Table XVIII lists E_{3j-1}, the Gaussian half-width for the various reflections as a function of time. For the reflections 333, 511, and 622, which have appreciable resolution, the Gaussian half-width listed is the simple addition of the resolved $K_{\alpha 1}$ and $K_{\alpha 2}$ half-widths. Figures 38 through 44 are the plots of the data of Table IX for each of the reflections. The relationship y = a + bx is least-squares fitted to the data of each of the reflections and the constants are listed in Table XVIII.

Table XVII

GAUSSIAN HALF-WIDTH $^{\circ}2\theta$ AS A FUNCTION OF TIME AFTER ANNEALING

Time, weeks	Reflection					
	111	200	220	311	333, 511	622
4, 5, 6	0.093±1	0.092±4	0.113±3	0.122±3	0.151±17	0.283±14
7, 8, 9	0.095±1	0.089±4	0.114±3	0.118±3	0.162±14	0.266±18
10, 11, 12	0.094±1	0.090±4	0.112±3	0.120±3	0.166±15	0.272±17
13, 14, 15	0.094±1	0.089±4	0.116±3	0.118±3	0.152±12	0.249±18
16, 17, 18	0.092±1	0.096±4	0.109±3	0.118±3	0.165±14	0.277±20
19, 20, 21	0.095±1	0.092±4	0.119±3	0.128±3	0.163±17	0.294±27
22, 23, 24	0.094±1	0.088±4	1.117±3	0.121±3	0.171±21	0.326±27
25, 26, 27	0.093±1	0.068±4	0.118±3	0.123±3	0.155±15	0.314±39
28, 29, 30	0.093±1	0.091±4	0.112±3	0.127±3	0.184±24	0.293±28

Table XVIII

COEFFICIENTS IN THE LINEAR EXPANSION y = a+bx FOR GAUSSIAN HALF-WIDTHS, $2\theta^{\circ}$, AS A FUNCTION OF TIME (IN WEEKS) FOR THE X-RAY REFLECTIONS EXAMINED FOR $^{238}PuO_2$

Reflection	a	b	
111	0.0941 ± 8	- 28 ± 45	* 10^{-6}
200	0.0913 ± 21	- 44 ± 116	
220	0.1124 ± 27	116 ± 144	
311	0.1172 ± 27	261 ± 143	
333, 511	0.1534 ± 68	464 ± 400	
622	0.2618 ± 131	1244 ± 897	

If, over a period of 30 weeks of observation, appreciable line broadening had occurred it is expected

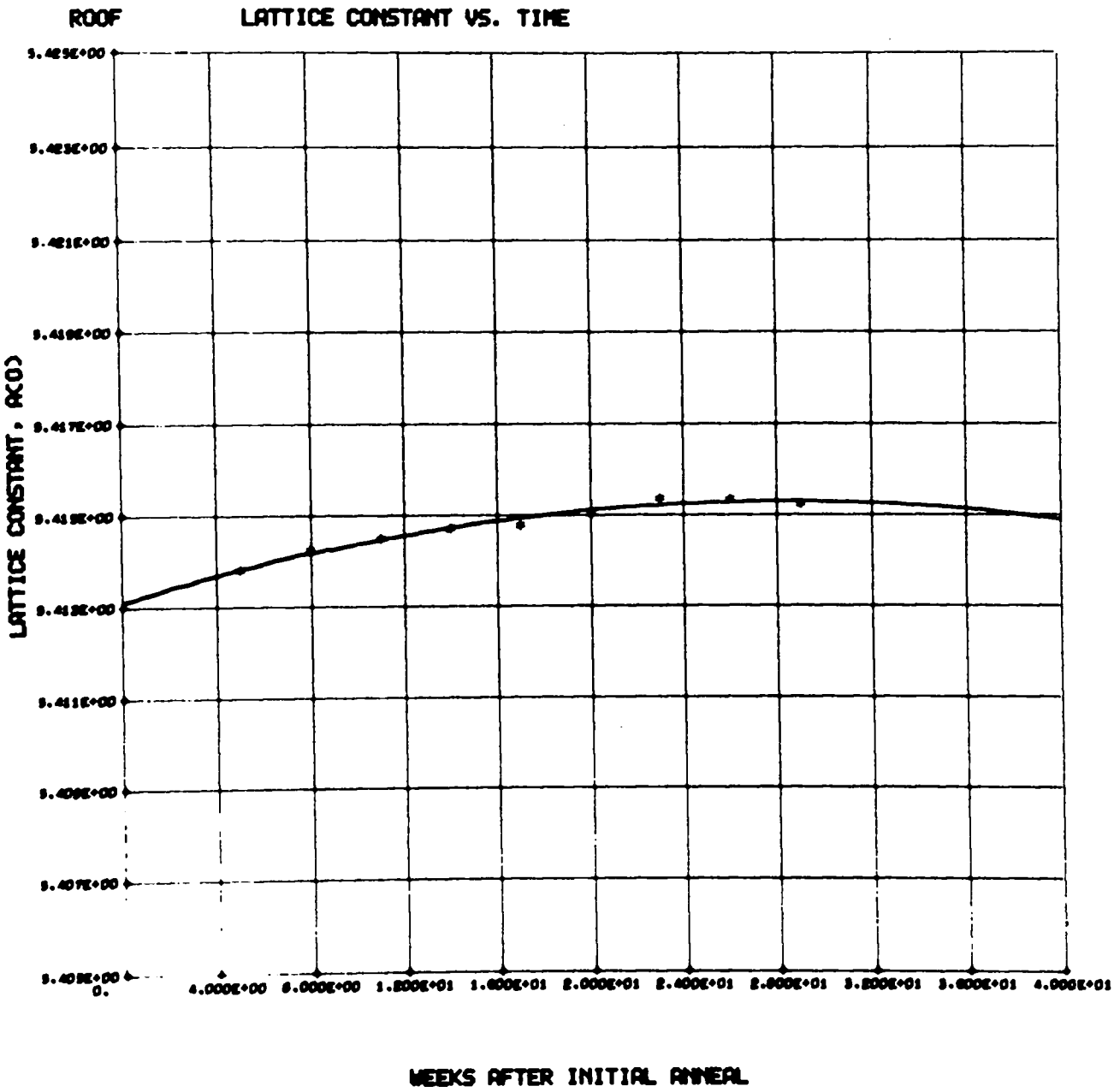

Fig. 36. Lattice Constant vs Time After Annealing for a Sample of $^{238}PuO_2$.

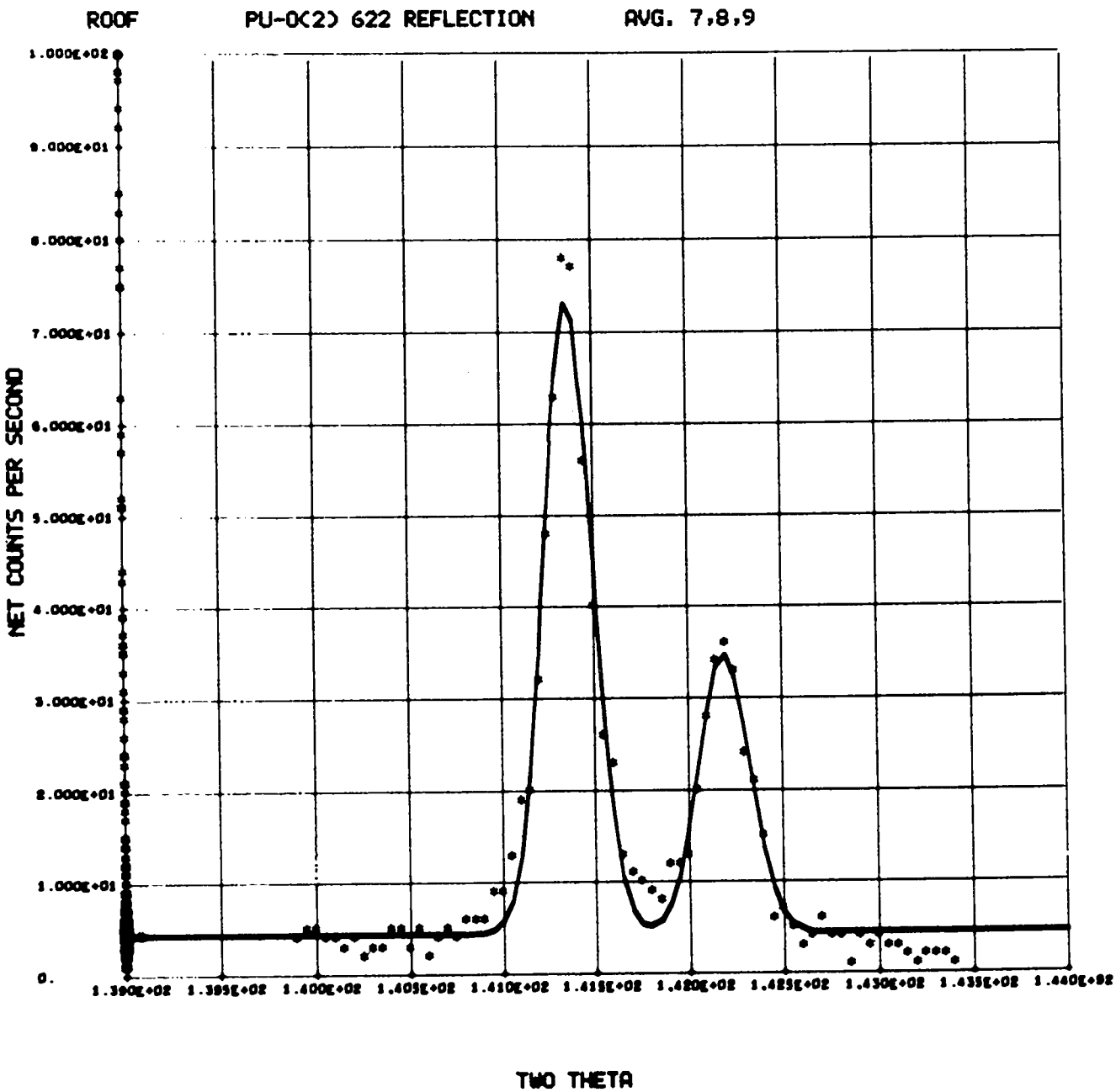

Fig. 37. The 622 Peak for a Sample of $^{238}PuO_2$ That Had Been Stored at Room Temperature for 7-9 Weeks After Being Annealed

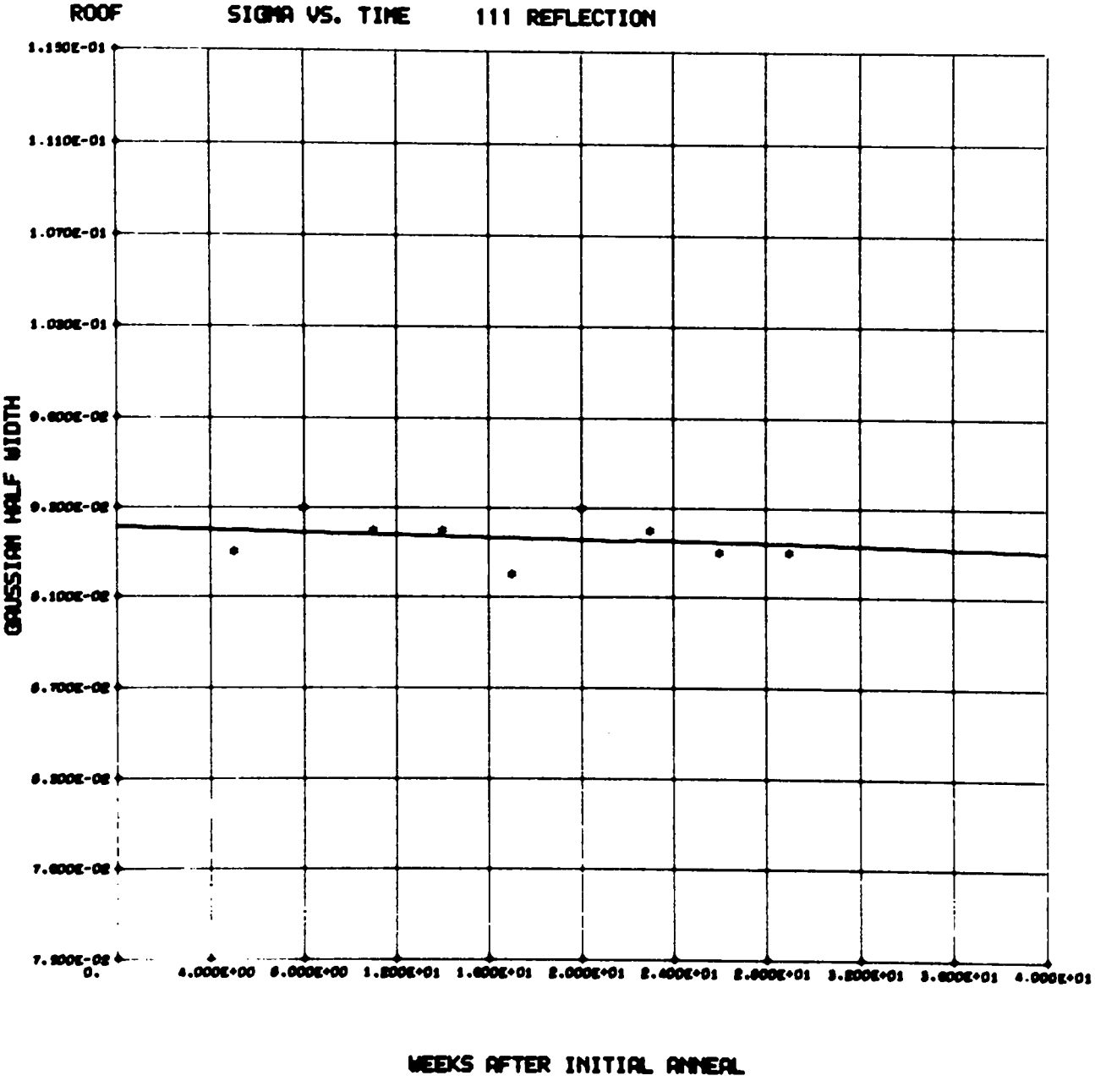

Fig. 38. Gaussian Half-Width vs Time After Annealing for the 111 Reflection of a Sample of $^{238}PuO_2$.

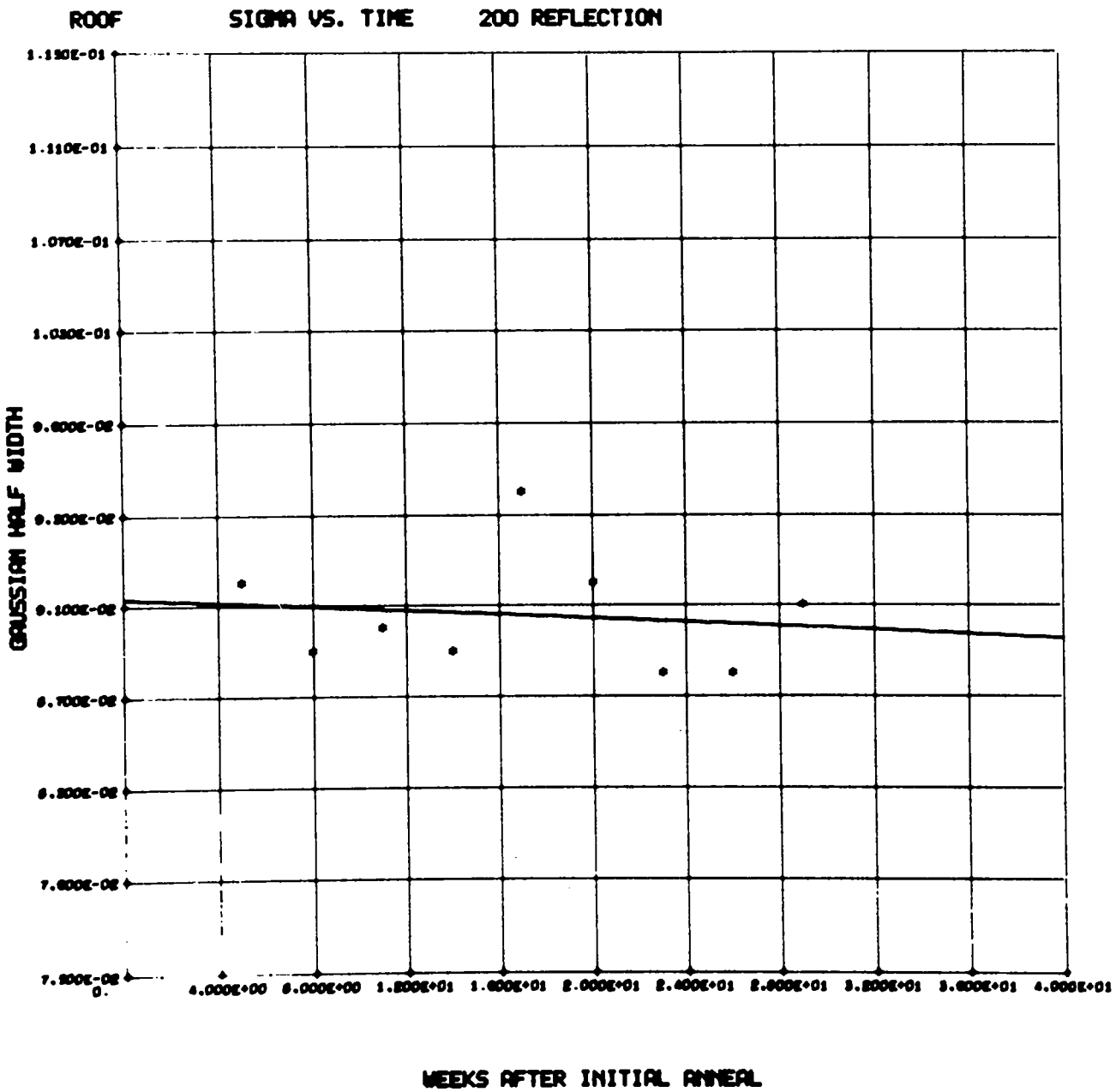

Fig. 39. Gaussian Half-Width vs Time After Annealing for the 200 Reflection of a Sample of $^{238}PuO_2$.

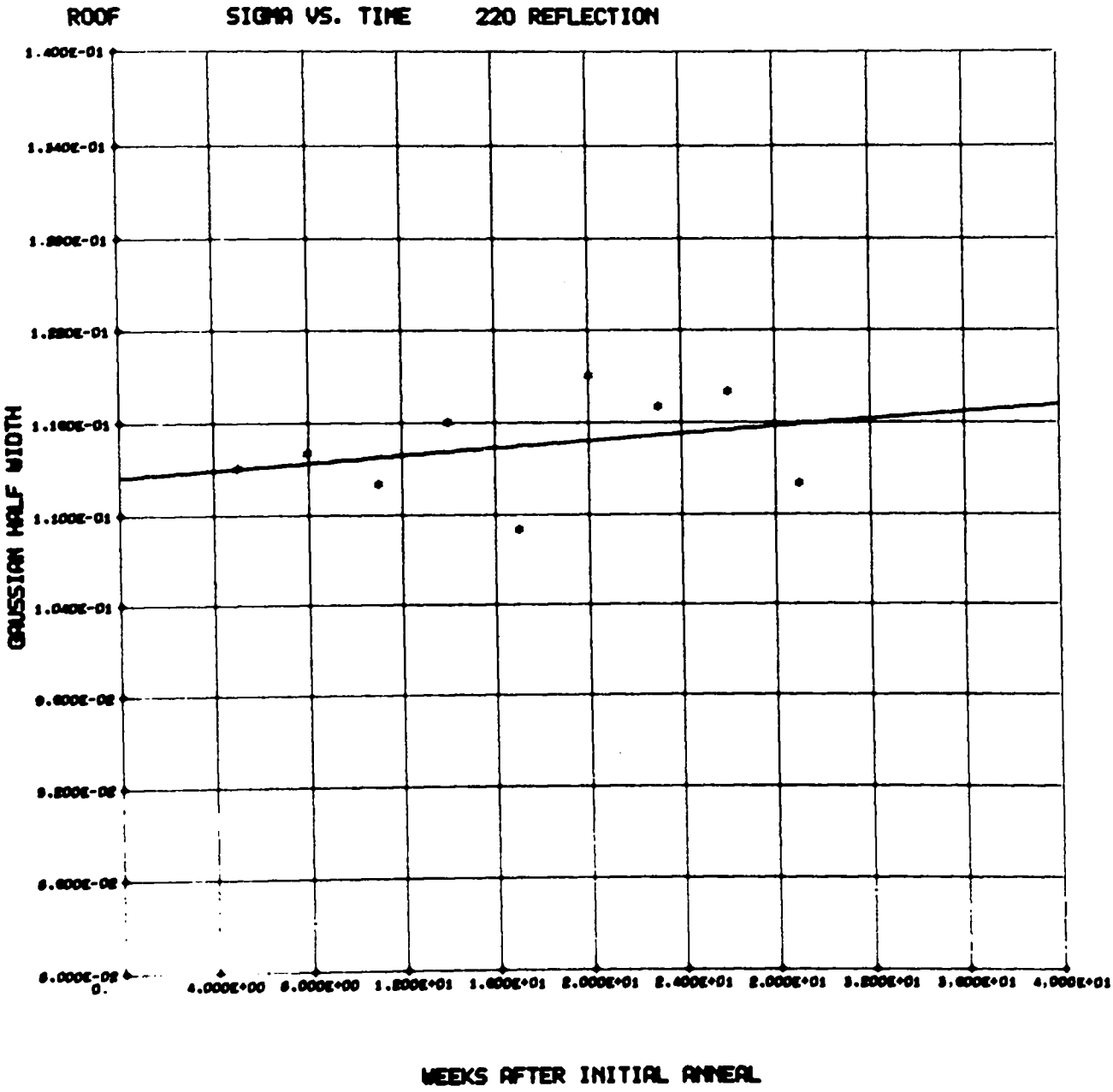

Fig. 40. Gaussian Half-Width vs Time After Annealing for the 220 Reflection of a Sample of $^{238}PuO_2$.

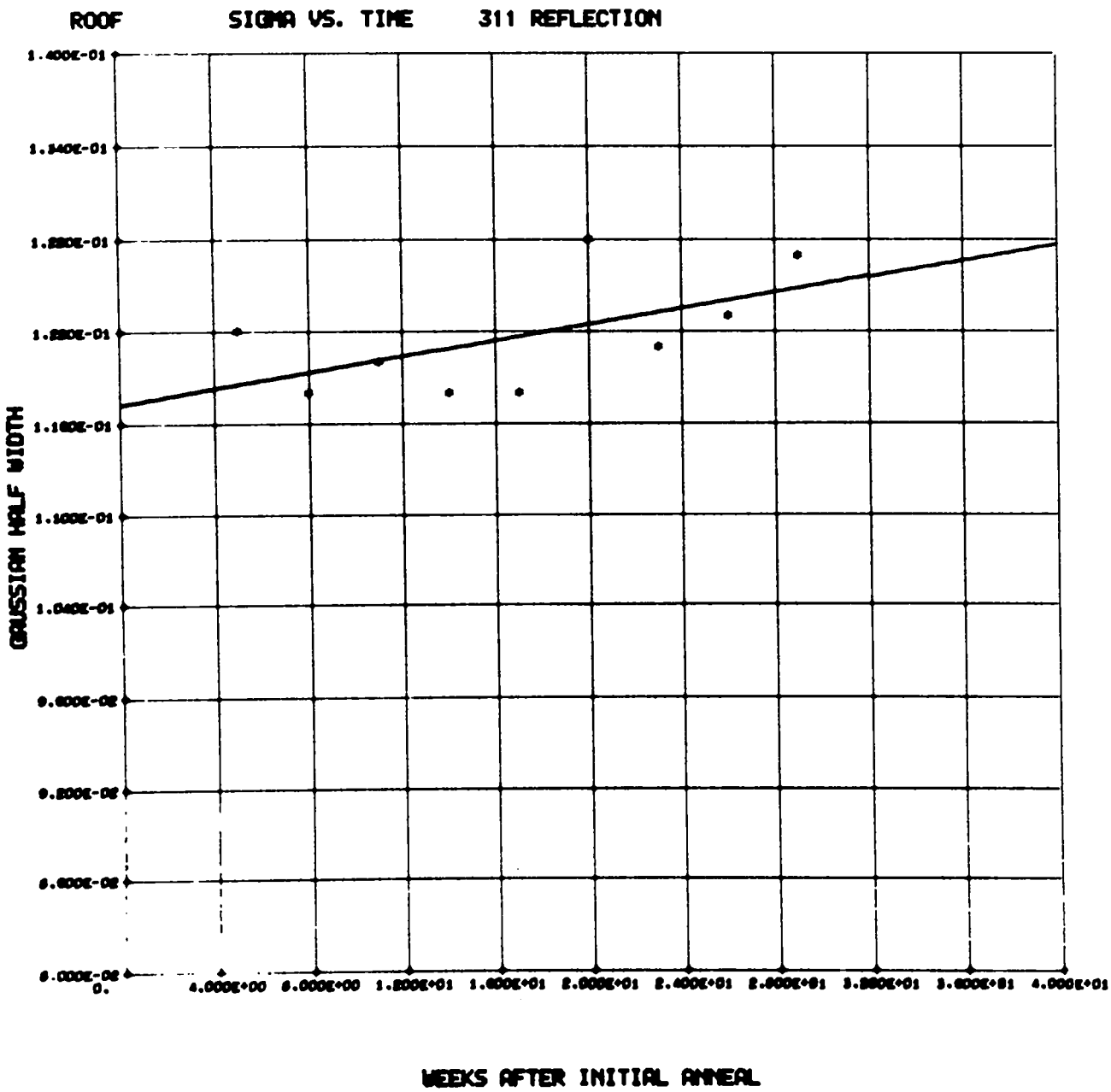

Fig. 41. Gaussian Half-Width vs Time After Annealing for the 311 Reflection of a Sample of $^{238}PuO_2$.

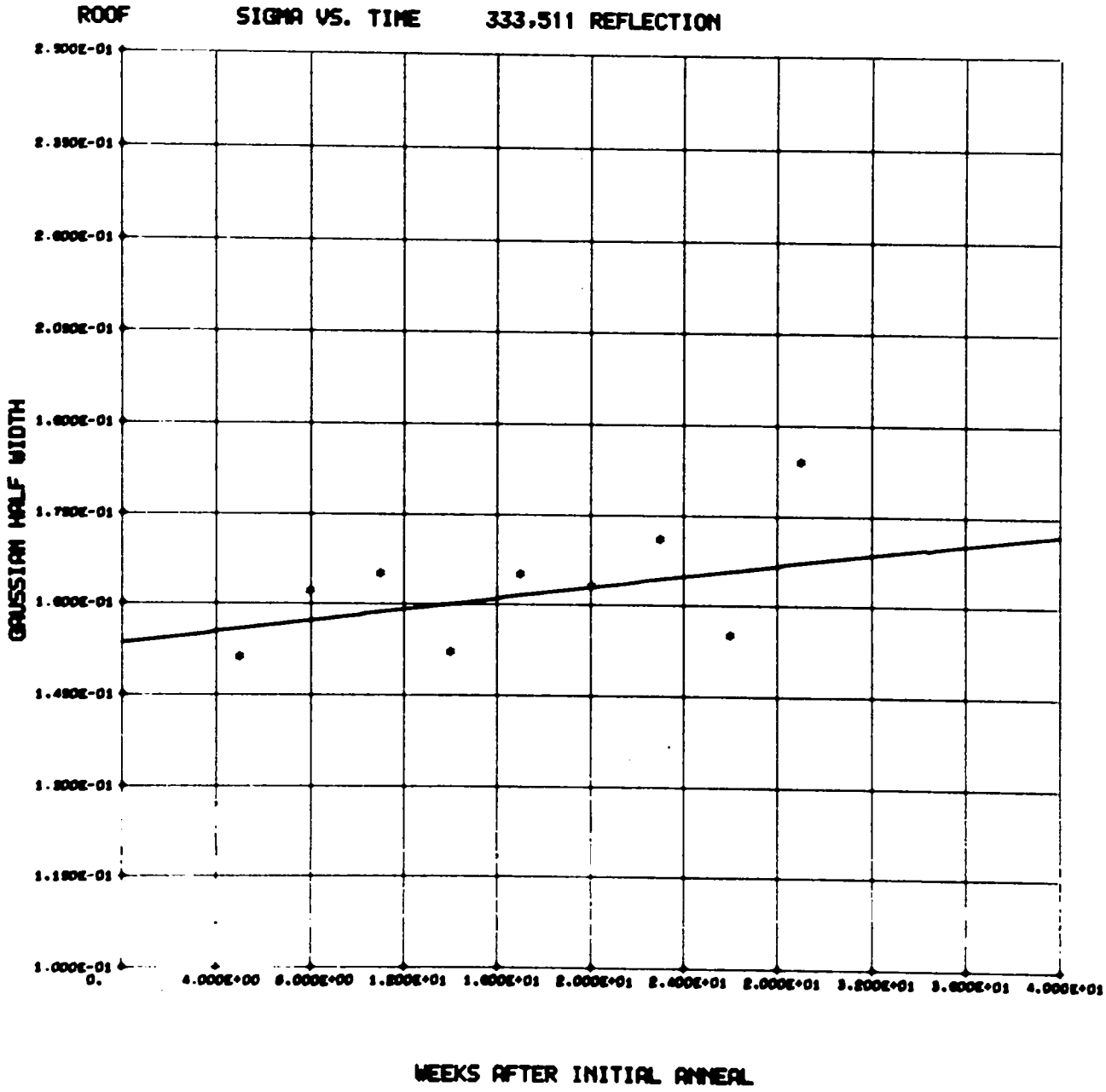

Fig. 42. Gaussian Half-Width vs Time After Annealing for the 333, 511 Reflection of a Sample of $^{238}PuO_2$.

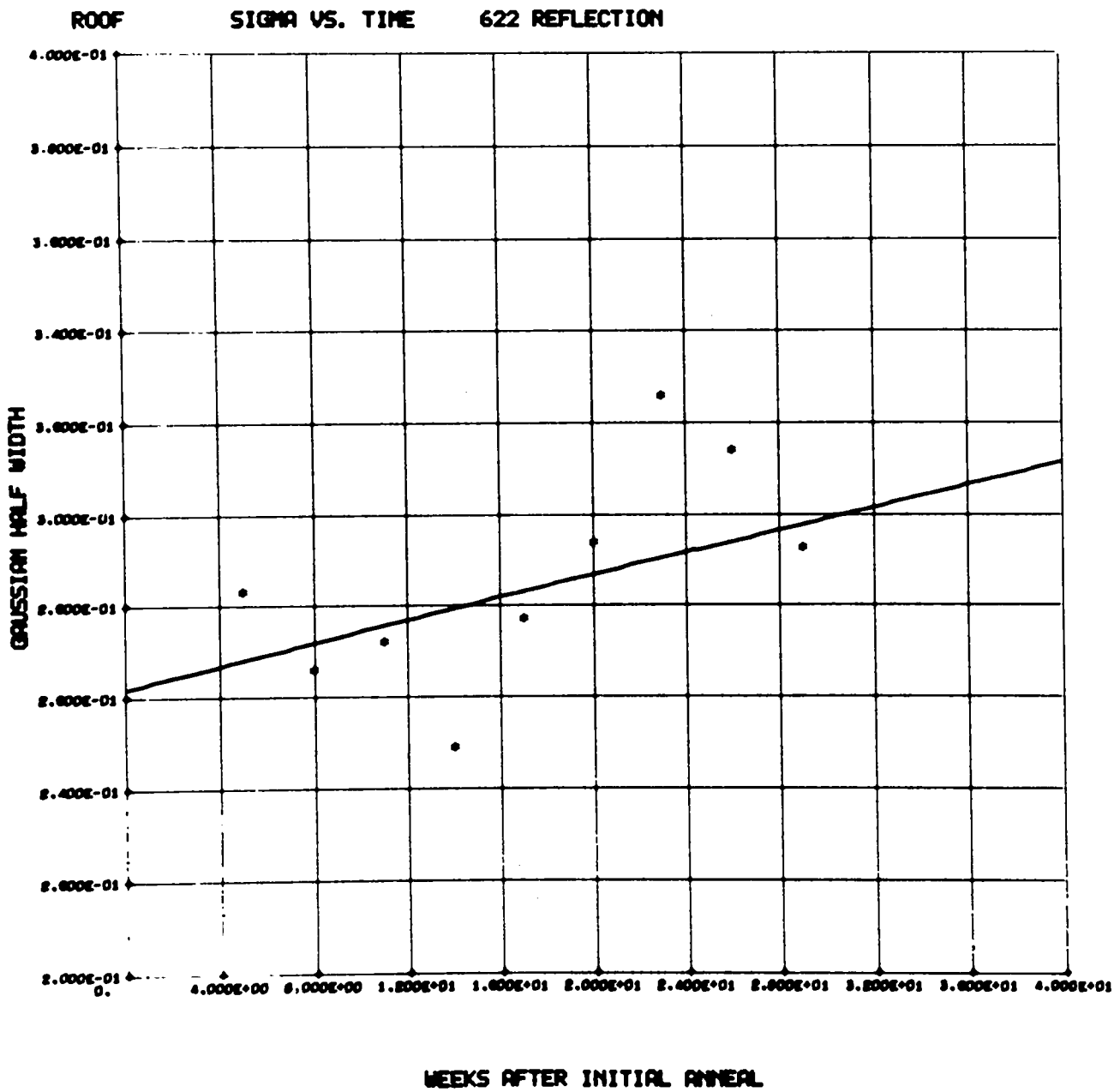

Fig. 43. Gaussian Half-Width vs Time After Annealing for the 622 Reflection of a Sample of $^{238}PuO_2$.

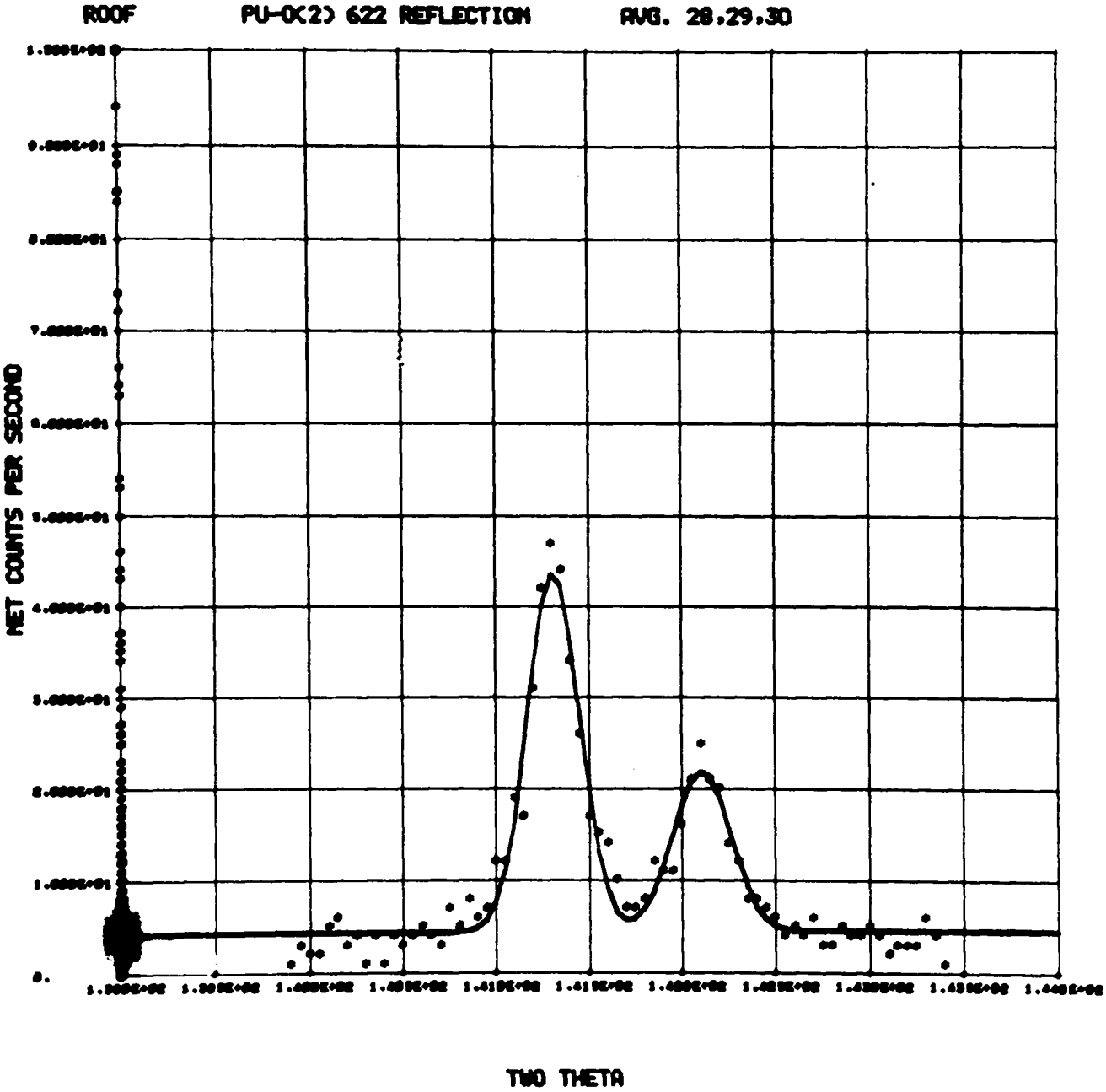

Fig. 44. The 622 Peak for a Sample of $^{238}PuO_2$ that had been Stored at Room Temperature for 28-30 Weeks After Being Annealed.

that the coefficient "b" of Table XVIII would be positive and significantly different from zero. While it may be argued that the data do not indicate significant difference from zero we believe that a trend is evident. For the higher order reflections the slopes are large and positive, and, if extrapolated, would predict an increase in the Gaussian half-width of about 0.1 $^{o}2\theta$ in 50 to 75 weeks from the time of an initial stress relief anneal. Figure 33 presents the 622 reflection 28-30 weeks after initial anneal. Comparison with Fig. 37 reveals the shift in position of the peaks resulting in a different lattice constant. The total intensity has decreased but the $K_{\alpha 1}$, $K_{\alpha 2}$ separation is still well resolved and no significant broadening is observed. The disappearance of the valley between the two peaks will be the first visual evidence for line broadening, as opposed to the mathematical evidence from curve fitting.

An increase of 0.1 $^{o}2\theta$ in Gaussian half-width implies a 0.25 $^{o}2\theta$ increase in the integral breadth. This amount is approximately the minimum required increase to be observed if the computer program UNFOLD is to be used to determine reliably crystallite size and strain through the integral breadth, Fourier coefficient, and 2nd Moment about the centroid methods. (R. B. Roof, Jr.)

C. Helium Release Studies

Cermet Samples - One cermet pellet (specimen 12965) 1/4 in. dia x 1/4 in. thick has been used in helium release experiments. Although this sample was made early in the development program, and thus cannot be assumed to be representative of current cermet behavior, it has provided preliminary experience relevant to working with a cermet, and the results are reported below. A nominal 20^{o}/min temperature ramp experiment was run with one piece from the outside of the pellet. Rapid release began at 700^{o}C and most of the helium had been released before 1000^{o}C had been attained. This range of rapid release, which is the lowest we have seen, occurred about 250^{o} lower than the corresponding range for Lot 93 microspheres. An isothermal test was run at 950^{o}C with another piece of the outside of the pellet. In 1500 sec, about 50% of the release had occurred. Although metallographic results are not yet available for these samples, it is presumed that the surface of the pellet had reacted with carbon during hot pressing. This would alter the microstructure of the pellet and thus contribute to the rapid release of helium. The third piece, this time from the center of the pellet, was run isothermally at 900^{o}C. In 18,000 sec, 50% of the helium had been released, which is quite rapid in comparison with the results we have obtained with other samples of various kinds at that temperature.

The helium contents of the two samples used in the isothermal experiments were determined to be 0.095 and 0.086 cc g^{-1}. The amount generated since hot pressing had taken place is calculated to be 0.092 cc g^{-1}.

Three uncoated cermet pellets [12970 (17A), 12971 (16B), and 12982 (30B)] have been placed in long term anneal tests at 900^{o}C. The first two contain 18 w/o ThO_2 - 12 w/o Mo and have been in test for about 30 days; the third contains 10 w/o ThO_2 - 12 w/o Mo and has been in test for about 2 weeks. We plan to remove one of the pellets from test in December to examine its microstructure and determine its helium content. The other two pellets will be allowed to continue in test.

Long Term Anneal Samples - Two samples that had been in compatibility tests at 900^{o}C have now been assayed for helium content. One (12375 A), a 35 w/o ZrO_2 solid solution pellet that had been held at 900^{o}C for 6671 hours, was run in a 20^{o}/min temperature ramp experiment. The helium content was found to be 0.309 cc g^{-1}, as compared with 0.353 cc g^{-1} generated during the 372 days that had elapsed since the pellet was sintered. Thus, 0.044 cc g^{-1} were presumably released during the time at 900^{o}, which amounts to an average rate of about 10% of generation during the time at temperature. Extrapolation of data obtained previously for this material at higher temperatures indicates that the effective diffusion coefficient at 900^{o}C is so low that essentially no helium should have been released at that temperature. The fact that 10% was released suggests that some process other than that observed in the short-term, high temperature experiments must be operative.

The other sample (12668), 100% PuO_2 that had been held at 900°C for 4910 hours, was heated rapidly to 1422°C in an isothermal experiment. After it had been annealed at 900°C the pellet appeared to be sound, with no visible cracks or surface imperfections. During the 1422° heating, however, it shattered violently into fragments ranging in size from fine powder to pieces large enough to weigh 0.2 g. The helium inventory was either 0.203 or 0.245 cc g^{-1} depending on whether it is assumed that the pellet shattered and was thrown out of the crucible after or before the helium was released. (Exactly when the shattering occurred is not known.) The calculated total amount generated during the 280 days since the sample was sintered is 0.409 cc g^{-1}. Assuming that the difference between the amount generated and the amount found represents release during the 900° anneal, the average release rate during the 205-day anneal was 0.6 or 0.7 of the generation rate. Extrapolation of high-temperature data for 100% PuO_2 pellets predicts no release at 900°C. The most probable interpretation of these contradictory results is that the temperature dependence of the effective diffusion coefficient exhibits a slope discontinuity resulting from the presence of two processes having different activation energies.

Aging Effects - Another pellet (12700) of 100% PuO_2 from the "new batch" (received in April 1969) was run in an isothermal test at 1475°C for comparison with data obtained previously (see Quarterly Report for July 1 - September 30, 1969, LA-4328-MS). The age of the pellet at the time of test was 159 days, and the time determined for 50% release was 281 sec. The effective diffusion coefficient computed from the 50% release time is $11.1 \times 10^{-5} sec^{-1}$. This result confirms the earlier conclusion that the new batch of material exhibits considerably faster release than does the old.

Long Term Data Analysis - Experiments so far performed have all been short term, in the sense that the generation of helium in the sample over periods of a day or so could be neglected. Now, however, longer tests are in progress, and diffusion equation solutions which take helium generation into account are desirable for data analysis. The generation rate of the helium, which is formed by radioactive decay, follows the decay laws, but, since the half life of the ^{238}Pu isotope is 89 years, the generation rate for periods shorter than 2 years may be taken as constant with negligible error. The differential equation is derived from Fick's law, assuming spherical geometry. This is the most useful case, since results for many geometries may be closely approximated by the results for a sphere, if an appropriate effective radius is used.

The differential equation is:

$$\frac{\partial C}{\partial t} = D\left(\frac{\partial^2 C}{\partial r^2} + \frac{2}{r}\frac{\partial C}{\partial r}\right) + B,$$

where C is concentration, t is time, D is the diffusion coefficient, r is the radial coordinate, and B is the generation rate. A constant concentration C_o is assumed as an initial condition, and a boundary condition or zero surface concentration is used, as it has been previously shown that this is appropriate for vaporization of helium at the surface. Thus $C(r, o) = C_o$ and $C(a, t) = 0$, where a is the sphere radius. The problem may be solved by conventional methods to give C as a function of radial coordinates and time:

$$C(r,t) = -\frac{2C_o a}{\pi r}\sum_{n=1}^{\infty}\frac{(-1)^n}{n}\sin\frac{n\pi r}{a}e^{-n^2\pi^2 Dt/a^2} + \ldots$$

$$\ldots + \frac{2Ba^3}{D\pi^3 r}\sum\frac{(-1)^n}{n^3}\sin\frac{n\pi r}{a}e^{-n^2\pi^2 Dt/a^2} + \ldots$$

$$\ldots + \frac{B}{6D}(a^2 - r^2) \quad .$$

This gives the concentration within the sphere. Of more interest is the quantity of helium retained by the sphere, which is found by integrating C(r, t) over the sphere volume. The result is:

$$\frac{Q}{Q_o} = \frac{6}{\pi^2}\sum_{n=1}^{\infty} n^{1/2} e^{-n^2\pi^2 Dt/a^2} - \ldots$$

$$\ldots - \frac{B}{D'C_o}\frac{6}{\pi^4}\sum_{n=1}^{\infty} n^{1/4} e^{-n^2\pi^2 Dt/a^2} + \frac{B}{15D'C_o},$$

where Q is the quantity of helium in the sphere at time t, Q_o is the initial helium content, and $D' = D/a^2$. Thus, Q/Q_o is the fraction of the initial helium content

remaining in the sphere.

Some properties of this result are: (1) For infinite time, $Q/Q_o = B/15D'C_o$; this giving the steady state helium content. (2) For short times (i.e. $Dt/a^2 < 10^{-4}$), the second and third terms cancel, leaving the solution obtained previously when generation was neglected. (3) The result is the fraction retained as a function of time, with D' ($= D/a^2$) and C_o as variable parameters; B is a fixed constant for any given material. (4) The equation cannot be solved explicitly for t, thus the time required to reach some predetermined helium content cannot be easily calculated, except by trial and error.

The results of a sample calculation, using values for C_o and B which are applicable to a long term anneal experiment presently in progress, are given below.

Sample Calculation - Two pellets containing 71.1 w/o PuO_2 have been put into isothermal test at 900°C. The pellets were 38 days old (elapsed time since hot pressing) and thus are presumed to contain 0.043 cc g^{-1} of helium at the time they were brought to 900°C. Table XIX shows the expected helium content after 30 and 60 days of annealing time for various values of D/a^2, as calculated on the basis of the foregoing equation. Table XIX shows that the helium will essentially all be released within 30 days for $D/a^2 = 10^{-6}$, but that for $D/a^2 \leq 10^{-8}$ the helium content will increase during the test. Since the generation rate is 0.0011 cc g^{-1} day^{-1}, it is evident that, if $D/a^2 \leq 10^{-9}$, it will take more than 750 days to reach the steady state helium content (which will be quite high). It should be emphasized that the data in Table XIX are applicable only for the particular value of 0.043 cc g^{-1} for the initial helium content. Other starting contents will give different results. The final, steady state content, however, will not change since it is a function only of the generation rate and D/a^2.

Table XIX

CALCULATED HELIUM CONTENTS AFTER 30 AND 60 DAYS FOR VARIOUS VALUES OF D/a^2

D/a^2	Helium content (cc g^{-1})			
	0 days	30 days	60 days	∞[a]
10^{-6}	0.043	0.0009	0.0009	0.0009
10^{-7}	0.043	0.010	0.009	0.009
10^{-8}	0.043	0.045	0.054	0.087
10^{-9}	0.043	0.066	0.090	0.867

[a]Steady state helium content.

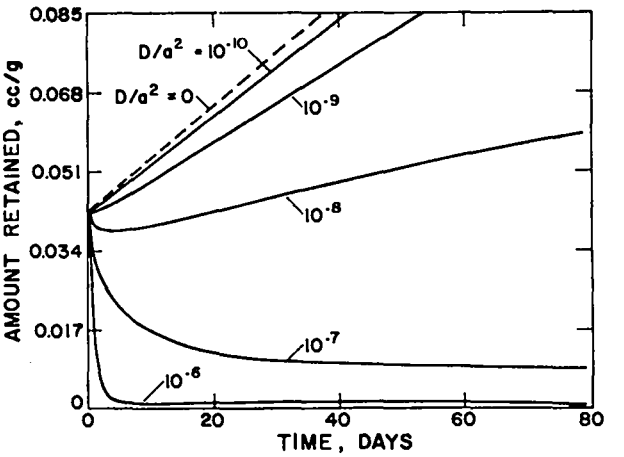

Fig. 45. Helium Content as a Function of Time for Various Values of D/a^2 (for 0.043 cc g^{-1} starting concentration).

Two parametric plots, Figs. 45 and 46, show the helium content of the sample as a function of time with various values of D/a^2, for starting concentrations of 0.043 and 0.5 cc g^{-1}, respectively.

It can be seen from the foregoing that the long term helium release situation can be characterized by three regimes; one with $D/a^2 < 10^{-9}$, another with $D/a^2 > 10^{-7}$, and the third with D/a^2 in the critical range between 10^{-7} and 10^{-9}. In the first case, little or no helium can be released, and the concentration will increase at some rate close to the generation rate. In the second, all the helium will be released during the first week or so, and, even after very long times, the helium content will be low. In the third case, where D/a^2 is in the critical range, exact prediction of the helium release behavior will be difficult because the results are sensitive to

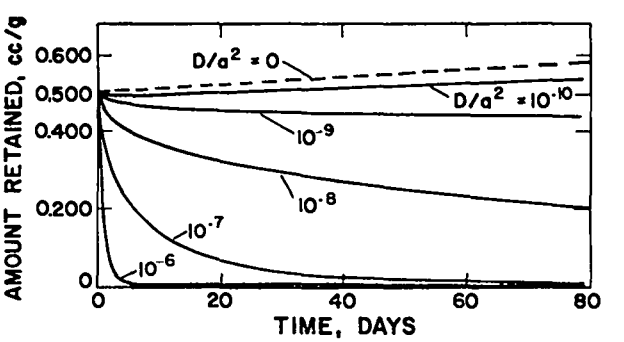

Fig. 46. Helium Content as a Function of Time for Various Values of D/a^2 (for 0.5 cc g^{-1} starting concentration).

small changes in D/a^2.

Thus, a rough prediction of helium release behavior over long times may be made from knowledge of the regime in which D/a^2 falls, the value of D/a^2 being determined by the combination of temperature and fuel material. (R.N.R. Mulford)

VI. MEETINGS

A. October 8, 1969: A program review was held at LASL. The status of the SSC fuel form was review for representatives of AEC/SNS/SEPO, MRC, AEC/DAO, and AEC/ALO.

B. October 23, 1969: T.K. Keenan attended a capsule review meeting at AEC/ALO and presented some SSC data to representatives of AEC/SNS, AI, MRC, ORNL, II, SL, TRW, and GE-Valley Forge.

C. November 3, 1969: T.K. Keenan attended a capsule design meeting at TRW. The results of the early Task 8 impact tests were discussed. A final overall 800 watt fuel dimension of "X" ± 0.050 in. and a final fuel power density of 3.2 w/cc was accepted by LASL. Personnel from AI, SL, and MRC also attended this meeting.

D. November 20-21, 1969: M.W. Shupe and T.K. Keenan attended the Third Meeting of the Isotope and Fuels Committee at MRC.

E. December 3, 1969: A program review was held at LASL for AEC/SNS/SEPO. Representatives from AEC/ALO and MRC also attended.

VII. SIMULANTS

Production of simulant discs during this quarter was considerably slower then the schedule proposed by GE-Evendale. In addition, the vendor experienced difficulty in meeting the specified dimensions and densities. GE proposed the addition of 0.67 w/o CaO to improve the low densities. This change was allowed after extensive discussions with TRW, AI, II, and AEC/SNS.

Table XX shows the consignment of simulant discs to December 31, 1969.

Other problems with simulants involved outgassing of discs (and embrittlement of capsule liner materials) when capsules were subjected to a re-entry environment thermal soak prior to impact testing. The problem did not lend itself to straightforward solution since the precise history of a specified set was not a matter of record.

Table XX

DISTRIBUTION OF SIMULANT DISCS THROUGH DECEMBER 31, 1969

Consignee	"As Sintered" Discs	Standard Overcoated Discs	Total
Atomics International	279	279	558
Isotopes, Inc.		130	130
MRC		105	105
LASL		14	14
			807

Analytical chemistry on QC discs supplied by GE yielded the following data:

Table XXI

A. CHEMICAL COMPOSITION OF TYPICAL NON-CALCIA DISC

Element	Amount
Th	75.8 w/o
Mo	13.5 w/o
C	75 ppm
H	20 ppm

Table XXII

B. SPECTROGRAPHIC ANALYSIS OF TYPICAL NON-CALCIA DISC

Element	Amount, ppm
Li	< 0.1
Be	< 4
B	< 0.5
Na	< 7
Mg	< 10
Al	10
Si	20
P	< 50
Ca	< 10
V	< 50
Cr	< 2
Mn	< 1
Fe	10
Ni	5
Cu	2
Zn	< 10
Ag	1
Cd	< 1
Sn	< 1
Pb	< 1
Bi	< 1

Table XXIII

C. OUTGASSING OF TYPICAL OVERCOATED NON-CALCIA DISCS

Treatment	Weight Loss, w/o, average of 5 Discs
1000°C, 1 hr in argon	0.031 (Range 0.0075-0.046)

More elaborate outgassing experiments to determine the nature of the emitted gasses have been in progress at other installations. When additional data have been collected and evaluated, a procedural specification for adequate outgassing can be written.

VIII. MILESTONES

The following milestones were attained during this report period:

Task V.2	Product Characterization
Task VI.1	Characterization of Small Specimens (except for data from other laboratories and aging effects)
Task VI.3	Large Disc Fabrication

IX. REFERENCES

1. M. Hansen, "Constitution of Binary Alloys", 2nd ed. McGraw Hill, New York (1958).
2. R.P. Elliott, "Constitution of Binary Alloys", 1st Supplement, McGraw Hill, New York (1965).
3. F.A. Shunk, "Constitution of Binary Alloys", 2nd Supplement, McGraw Hill, New York (1969).
4. Y. Adda, J. Philibert, "La Diffusion dans les Solids", Presses Universitaires de France, Paris (1966).
5. Diffusion Data, Diffusion Information Center, Cleveland, Ohio, USA.
6. R. Resnick, L.S. Castleman, Trans. AIME 218 (1960) 307.
7. T.S. Lundy, F.R. Winslow, R.E. Pawel, C.J. McHargue, Trans. AIME 233 (1965) 1533.
8. E. Gebhardt, K. Kirner, Z. Metallkunde 54 (1963) 437.
9. J. Askill, D.H. Tomlin, Phil. Mag. 8 (1963) 997.
10. J. Askill, "Diffusion in Body Centered Cubic Metals", ASM, Metals Park (1965) 247.
11. L.S. Birks, R.E. Seebold, J. Nuclear Mat. 3 (1961) 249.
12. D.A. Prokoskin, E.V. Vasileva, L.L. Vergasova, Metalloved. Term. Obrab. Metall (1967) No. 3 44-6.
13. J.A.M. van Liempt, Rec. Trav. Chem. Pays-Bas 51 (1932) 114.
14. J. Askill, Phys. Stat. Sol. 23 (1967) p 21-23.
15. S.Z. Bokshtein, M.B. Bronfin, S.T. Kishkin, "Diffusion Processes, Structure, and Properties of Metals", Consultants Bureau, New York (1965) p 16 and 24.
16. R.L. Eager, D.B. Langmuir, Phys. Rev. 89 (1953) 911.
17. R.E. Pawel, T.S. Lundy, Acta Met. 13 (1965) 345.
18. R.E. Pawel, T.S. Lundy, J. Phys. Chem. Solids 26 (1965) 937.
19. I.A. Tregubov, L.N. Kuzina, O.S. Ivanov, Doklad. Akad. Nauk USSR 180 (1968) 423-4.
20. W. Danneberg, Metall W. und Tech. 15 (1961) 977.
21. R.E. Pawel, T.S. Lundy, J. Electrochem. Soc. 115 (1968) 233-7.
22. L.N. Larikov, V.M. Tyskevich, L.F. Choma, Ukr. Fiz. Zh. 12 (1967) 983-7.
23. E.V. Borisov, P.L. Gruzin, S.V. Zemskii, Zashch. Pokryt. Metal. No. 2 (1968) 104-9.
24. K. Mendelssohn, E. King, J.A. Lee, M.H. Rand, C.S. Griffin, and R.S. Street, in Plutonium 1965, A.E. Kay and M.B. Waldron, Eds., Chapman and Hall, London (1967) p 201.